CHEMICAL AGENT INDUCED REDUCTION OF SKIN LIGHT SCATTERING

A Dissertation

by

JASON M. HIRSHBURG

Submitted to the Office of Graduate Studies of
Texas A&M University
in partial fulfillment of the requirements for the degree of

DOCTOR OF PHILOSOPHY

December 2009

Major Subject: Biomedical Engineering

CHEMICAL AGENT INDUCED REDUCTION OF SKIN LIGHT SCATTERING

A Dissertation

by

JASON M. HIRSHBURG

Submitted to the Office of Graduate Studies of
Texas A&M University
in partial fulfillment of the requirements for the degree of

DOCTOR OF PHILOSOPHY

Approved by:

Chair of Committee,	Alvin T. Yeh
Committee Members,	Gerard L. Coté
	Melissa A. Grunlan
	Andreas Holzenburg
	J. Stuart Nelson
Head of Department,	Gerard L. Coté

December 2009

Major Subject: Biomedical Engineering

ABSTRACT

Chemical Agent Induced Reduction of Skin Light Scattering. (December 2009)

Jason M. Hirshburg, B.E., Vanderbilt University

Chair of Advisory Committee: Dr. Alvin T. Yeh

Skin turbidity limits light based medical applications while increasing the risk of epidermal thermal injury. Collagen fibers are responsible for the majority of light scattering within skin. Chemicals, known as clearing agents, reduce tissue light scattering with the potential to increase the efficacy of light based imaging and therapeutic applications. Three hypotheses have been suggested for the clearing mechanism: index of refraction matching between clearing agent and collagen, tissue dehydration, and agent induced collagen structure perturbation. This study investigates optical clearing in skin while presenting a comprehensive clearing mechanism.

Clearing was found to be a complex process with thermodynamic and kinetic components. Concentration gradients drive clearing agents to diffuse into skin and remove water. The introduction of clearing agents into the tissue reduces light scatter. The speed of clearing was found to increase with molecular size and number of hydroxyl groups.

The molecular modeling program CHARMM suggests collagen affinity plays a major role in clearing agents' ability to interact with collagen and remove bound water. Collagen solubility is a measure of clearing agent affinity for collagen and was found as

a predictor of agent clearing potential. Increasing agent molecular size led to a greater reduction of fibrillogenesis with corresponding high collagen solubility.

Raman spectroscopy quantified clearing agent induced dehydration of dermal collagen. Clearing agent ability to dehydrate dermal collagen corresponded with collagen affinity and the ability to clear tissue optically. The most effective clearing agents were found to remove bound water with the greatest efficacy.

Replacement of collagen triple helix bound water by clearing agents with an index of refraction similar to collagen optically homogenizes skin tissue leading to a reduction in light scattering. Through dehydration of collagen with concomitant diffusion of clearing agent into collagen, the skin is homogenized leading to a large reduction in tissue light scattering.

ACKNOWLEDGEMENTS

I would like to thank my adviser Alvin Yeh for his guidance and support over the last five years of study at Texas A&M University. Special thanks also go to my committee members J. Stuart Nelson, Gerard Coté, Melissa Grunlan, and Andreas Holzenburg. My parents Ed and Linda, my brothers Jeff and Keith, and friends have encouraged, supported, and made graduate school a wonderful experience.

TABLE OF CONTENTS

CHAPTER Page

LIST OF FIGURES

FIGURE Page

FIGURE Page

LIST OF TABLES

CHAPTER I

INTRODUCTION

1.1 Brief Review of Optical Clearing

The turbidity of most biological tissue limits biomedical applications of light-based diagnostics and therapeutics. Multiple scattering events reduce the effective depth over which information about the tissue can be ascertained and the ability to localize embedded features of interest. Optical imaging of deep structures is difficult due to the rapid degradation of image resolution and signal strength with increased depth. Furthermore, optical scattering restricts delivery of a collimated laser beam to subsurface targets such as blood vessels, decreasing the efficacy of light-based therapeutic applications.

Prior studies demonstrate that a reduction in optical scattering can improve the efficacy of light-based techniques in medical applications[1-9]. Non-reactive chemical agents, in particular sugars (e.g., glucose) and sugar-alcohols (e.g., glycerol) have been used to temporarily increase tissue transparency[1-3-10-12]. These agents have been investigated primarily in collagenous tissues with initial studies measuring induced increases in light transmittance in ocular sclera[1].

This dissertation follows the style of Lasers in Surgery and Medicine.

In fact, agents have been shown to be most effective when applied directly to the mesenchyme of tissue systems such as the dermis of skin. Application of glycerol sub-dermally in vitro or by injection in vivo reduced light scattering in skin, improved detection of fluorescence signal from subsurface targets and enhanced visualization of subsurface blood vessels[2-3]. This optical clearing effect has been studied in other tissue systems such as muscle[10] and the gastrointestinal tract[11] as well as used for agent sensing, where a reduction in tissue scattering occurred with increased blood glucose levels[6].

1.2 Significance and Identification of Opportunity

Development of topically applied clearing agents would have a large impact on a wide range of skin conditions and diseases. Many patients suffer from a considerable degree of psychological morbidity from these conditions further increasing the need for effective treatments[13]. Table 1 lists several dermatologic pathologic conditions that would benefit from clearing agents.

Table 1: Conditions currently treated with light based therapies that would benefit from clearing agents.

Vascular Lesions	Pigmented Lesions	Other Skin Pathologies
Port Wine Stain (PWS)	Lentigo	Skin Cancers
Hemangiomas	Nevus of Ota	Acne Vulgaris
Telangiectasias	Nevus of Ito	Acne Scars
Angiomas	Blue Nevus	Hypertrophic Scars
Adenoma sebaceum	Ephelides	Rhytides
Angiokeratomas	Becker's Nevi	Hypertrichosis
Venous Lakes	Hairy Nevi	Hidradenitis Suppurative
Spider Veins	Epidermal Melanosis	Pseudo-folliculitis Barbae
Rosacea	Nevus Spilus	Traumatic and Decorative Tattoos
Poikiloderma of Civatte	Mucocutaneous Hyper-Pigmentation	Chrysiasis

Many of the conditions listed in Table 1, such as Port Wine Stain (PWS) involve abnormal growth of tissues within and under the skin. PWS is a congenital malformation of the vasculature within skin that occurs in approximately 1,500,000 in the United States and thirty-two million people worldwide[14-16]. PWS is more than a cosmetic problem; personality development is adversely affected in PWS patients with detailed studies documenting low self-esteem and problems with interpersonal relationships[17-19]. PWS is characterized by flat, red macules that darken and become raised over time due to the development of vascular nodules (Figure 1)[20-21].

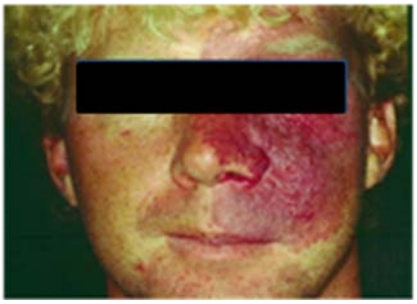

Figure 1: Twenty-four year old Caucasian male with PWS.

Studies of PWS show a normal epidermis overlaying an abnormal plexus of dilated blood vessels within the dermis. Currently, pulsed dye lasers are used to destroy dermal blood vessels and are the therapy of choice for PWS. However, treatment success remains variable and unpredictable. Complete blanching of the lesions occur in only 10% of patients even after multiple laser treatments. This low success rate is caused by the light scatter within skin. The scattering reduces the ability of the laser to deliver an adequate amount of light to the targeted PWS blood vessels (Figure 2).

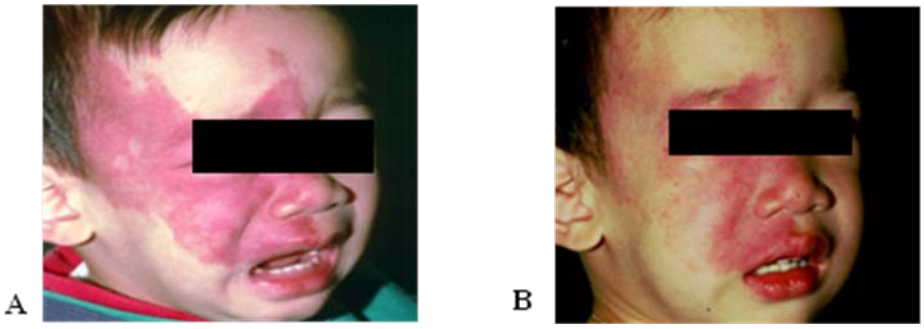

Figure 2: Two-year-old Asian male with PWS of the right face: (A) prior to laser therapy; and (B) two years after eight laser treatments.

The use of clearing agents to reduce the light scattering properties of skin would:

- Improve the effectiveness of the laser treatment
- Reduce the risk of burns to the patient
- Potentially reduce the number of required treatments lowering the cost and time of treatment.

1.3 Proposed Clearing Mechanisms

The turbidity of skin is due to light scattering associated with dermal collagen[22]. Thus the interaction of clearing agents and collagen play a central role in reducing light scattering within skin. Previous studies used common properties of these chemical agents to suggest that refractive index matching and dehydration are possible mechanisms for tissue optical clearing. Light scattering in dermis is predominantly from ubiquitous collagen fibers[22]. Indeed, all studies cited used agents with indices of refraction within the range reported for collagen (from 1.35 to 1.55)[2-3-8-22-27]. Dehydration is also believed to play a role as all reported agents are hyperosmotic with respect to biological tissue. However, these parameters, refractive index and osmolarity, do *not* correlate with agent optical clearing potential[27]. In fact, tissue optical clearing with glycerol shows a strong inverse dependence on the degree of covalent cross-linking present[28] and in vitro studies of collagen gel opacity correlated with sugar and sugar-alcohol concentrations[29] suggesting the importance of agent-collagen molecular interactions.

Molecular interactions of sugars and sugar-alcohols and their destabilizing and inhibitory effects on collagen structure and fibrillogenesis have been extensively studied within the biochemistry community. Such studies provide insight on a molecular mechanism of tissue optical clearing and a means of rational selection and design of effective chemical agents. This work examines the role refractive index matching, dehydration, and collagen structure perturbation play in bulk tissue clearing. A comprehensive clearing mechanism based on homogenizing the optical properties of skin through clearing agent removal of collagen's bound water is presented.

CHAPTER II

TISSUE OPTICS

2.1 Skin Anatomy

Skin consists of three layers: 1) the epidermis; 2) dermis; and 3) subcutaneous fat (Figure 3). The epidermis is the thinnest layer averaging 100 μm in thickness and is largely cellular. The most superficial layer is the stratum corneum (SC). The SC is responsible for the barrier effects of skin and consists largely of differentiated cells surrounded by a lipid membrane. Below the SC, the epidermis is metabolically active containing several cell types. Keratinocytes form the majority of the epidermis and contribute to SC formation. Melanocytes produce melanin, a chemical involved in skin pigmentation. Other cell types include Langerhans cells (immune function) and Merkel cells involved in touch perception.

Figure 3: The three layers of skin.

The dermis is largely connective tissue responsible for the mechanical properties of skin and consists of collagen and elastin. The small superficial portion of the dermis is called the papillary dermis and contains a loose network of small collagen fibers (0.3-3.0 μm diameter). Below the papillary dermis is the reticular dermis. The reticular dermis forms the majority of the dermis and is characterized by densely packed, large collagen fibers (10-40 μm diameter) oriented parallel to the skin surface. Surrounding the collagen is an amorphous ground substance consisting primarily of water. Below the dermis is a layer of subcutaneous fat.

2.1.1 Collagen Structure

An understanding of collagen structure is required due to the pivotal role it plays in dictating skin optical properties and clearing. Dermal collagen is primarily Type I collagen and is characterized by a structural hierarchy[30].

Primary structure describes the sequence of amino acids that form proteins. Collagen is a hydrophilic protein consisting of mostly acidic, basic, and hydroxylated amino acid residues. Glycine (GLY), shown in Figure 4 is the most common residue and is regularly spaced throughout the entirety of the molecule in GLY-X-Y repeats. Proline (PRO) and hyroxy-proline (HPO) are the next most abundant residues found in the “X” and “Y” positions, and constitute almost 25% of collagen’s primary sequence.

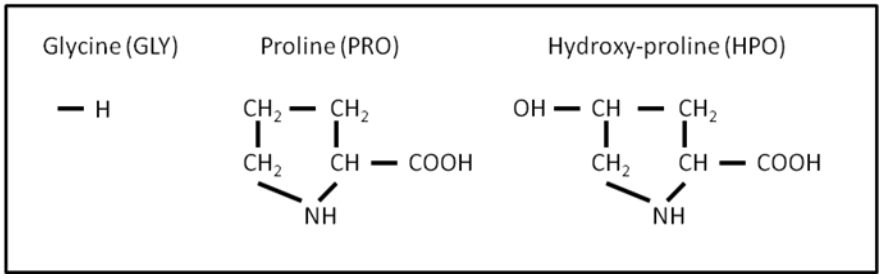

Figure 4: Structure of amino acids commonly found in collagen.

The secondary structure details the configuration of individual chains formed by the amino acid sequence. Type I collagen has a left-handed helical secondary structure with a pitch of about 9 Å. The occurrence of a glycine residue at every third position allows for sterically permissible hydrogen bonding.

Tertiary refers to the helicity or large scale folding by the totality of polymeric chains. The tertiary structure of collagen is a right handed triple helix which forms the fundamental molecular unit of collagen fibers (Figure 5A). The triple helix consists of three left handed helices with a repeat distance of 100 Å, a length of about 2800 Å and diameter of 15 Å. Of these helices two are identical and are known as α1 chains with the third chain being somewhat different and known as an α2 chain. The end of the triple helix is non-helical in nature and is thought to be the primary cite of crosslink formation with other triple-helices.

Quaternary structure refers to large scale aggregates of collagen triple-helices. Triple-helices combine to form collagen fibrils (Figure 5B,C). Attractive forces between triple-helices are largely hydrophilic in nature (hydrogen bonding) with some inter-helix covalent crosslink formation between non-helical regions. Fibrils show a banding

pattern of light and dark regions in electron microscopy images characteristic of the staggered nature of triple-helix aggregation. Dark regions are characteristic of complete overlap of collagen triple-helices forming the fibril. Light regions are areas that incorporate gaps between triple-helices. One fibril period or "repeat region" consists of one light region and one dark region and is about 680 Å in length.

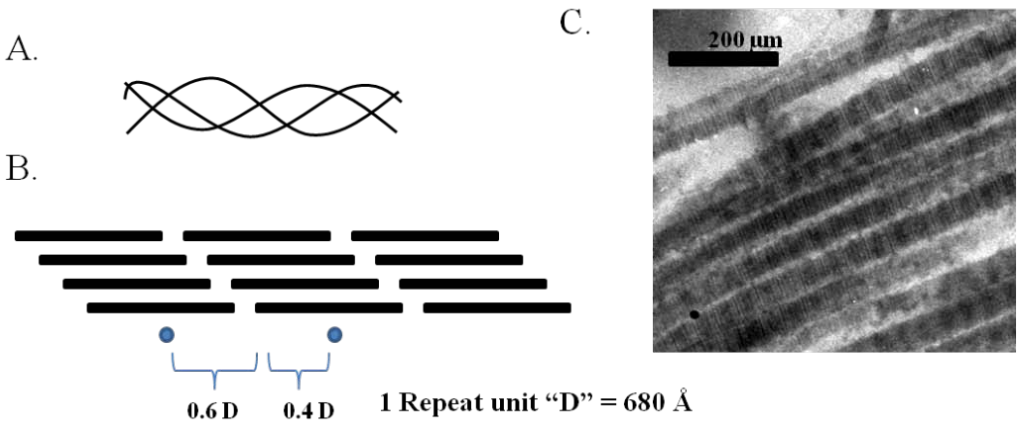

Figure 5: Tertiary and quaternary structure of collagen. (A) One repeat unit of triple helix; (B) Triple-helices aggregate forming collagen fibrils; (C) Transmission electron microscopy image of rodent tail collagen fibrils.

2.2 Optics of Bulk Skin

Light interaction with tissue can be quantitatively described by optical property coefficients (Table 2).

Table 2: Tissue optical property coefficients.

Event	Symbol [units]	Description
Absorption	μ_a	Photons eliminated by exciting matter
Scattering	μ_s	Light emitted from charge oscillations
Anisotropy	g	Average cosine of scattering angles
Reduced Scattering	$\mu_s' = \mu_s(1-g)$	Effective amount of scattering within tissue

Absorption and scattering contribute to tissue turbidity. Both the absorption and scattering coefficients have units of inverse centimeters (cm^{-1}) and quantify the average amount of absorptive or scattering events per unit length. Absorption is the transfer of energy from a photon to matter usually resulting in electrons raised to an excited state (Figure 6A). The increase in energy is dissipated through radiative events such as flouresence or non-radiative events such as heat. Absorption in skin is small relative to scattering and assumed constant with application of clearing agents (Table 3)[24].

Table 3: Optical properties of the epidermis and dermis.

Skin Layer	λ (nm)	μ_a (cm^{-1})	μ_s (cm^{-1})	g	n
Epidermis	633	4.3	107	0.79	1.5
Dermis	633	2.7	187	0.82	1.4

Scattering is large in skin compared with absorption and provides the principal contribution leading to tissue turbidity. Scattering results from the interaction of light with atoms and molecules. Light waves induce the electric charges of atoms and

molecules within the tissue to oscillate and emit secondary electromagnetic radiation. The emitted secondary radiation is considered light "scattered" by the material (Figure 6B). Scattering within tissue is usually quantified by the reduced scattering coefficient, μ_s'. μ_s' incorporates anisotropy, g, giving the scattering description a directional component and is commonly used rather than the scattering coefficient, μ_s. Anisotropy is a quantity that describes the direction of the scattered light.

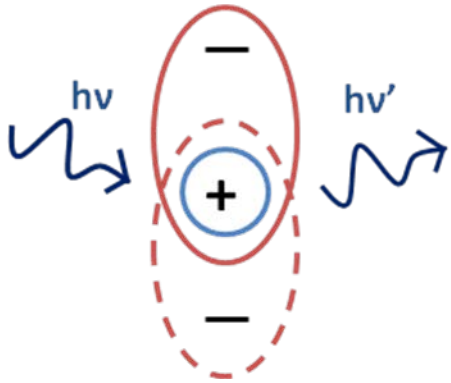

Figure 6: Light absorption.

2.3 Light Scattering from Collagen

Previous studies indicate that refractive index differences between collagen and the surrounding medium in skin lead to light scattering[1-24]. The scattering coefficients are useful for describing the amount of scattering events in bulk tissue as well as attenuation calculations for light propagation. When considering scattering of light waves with collagen, the index of refraction is useful.

2.3.1 Index of Refraction

Index of refraction is easily illustrated by reflection and refraction of incident light upon an optically smooth surface (Figure 7).

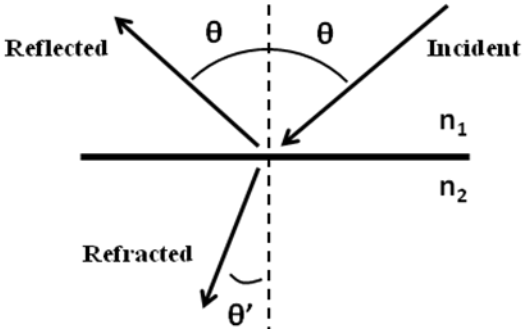

Figure 7: Reflection and refraction at a surface.

The directions of the reflected and refracted waves are described by the law of specular reflection and Snell's law. These laws express the direction of each light "ray" based on the index of refraction, n, of the medium. Figure 7 shows an example with conditions: $n_1 < n_2$ and $\theta' < \theta$. The larger refractive index n_2 has "bent" the light at the interface where the refracted light forms a smaller angle with the line normal to the surface. The magnitude of the "bend" varies with the ratio of each material's refractive index.

The example above can also be depicted by considering the molecular nature of matter. The homogenous, transparent medium with an index of n_2 is actually an aggregation of many molecules. As described in the above section, incident light waves create oscillations in molecules causing a secondary emitted electric field. Thus, each molecule is acted on by not only the incident light wave, but the emitted fields of the

surrounding molecules. The solution to this many body problem is illustrated by the bending of light at the surface resulting in the refracted ray. The net result is the superposition of the many secondary waves giving one refracted ray with a propagation velocity of c/n, where c is the speed of light and n is the refractive index. The incident wave is extinguished in the medium and outside the secondary waves give rise to the reflected ray. The index of refraction, n, is thus the expression of scattering by many small particles (molecules) that make up a medium and is dependent on the number of particles and their polarizability. In skin, light scattering is somewhat more complicated than the example above. However, differences between the refractive index of collagen fibers and surrounding medium give rise to many scattering events that lead to tissue turbidity.

CHAPTER III

BULK SKIN CLEARING

3.1 Measuring Optical Properties of Skin Using Inverse Adding-Doubling

The absorption and reduced scattering coefficients describe light attenuation in tissues. The inverse adding doubling method (IAD) is an effective and commonly used method to calculate each coefficient[22-24-31]. IAD uses total reflectance and total transmission to calculate the optical properties of bulk tissue. "Inverse" describes the reverse of the usual process of calculating reflection and transmission from optical properties. "Adding-doubling" indicates the way the radiative transport equation is solved within a specified error range. The radiative transport equation (RTE) describes light propagation within tissue. The overall equation is an energy balance in the form[24]:

$$\frac{\partial I(\boldsymbol{r},\boldsymbol{s})}{\partial \boldsymbol{s}} = -\mu_t I(\boldsymbol{r},\boldsymbol{s}) + \frac{\mu_s}{4\pi}\int_{4\pi} I(\boldsymbol{r},\boldsymbol{s}')p(\boldsymbol{s},\boldsymbol{s}')d\Omega' \qquad 3.1$$

[Change of energy of area element = Energy out + Energy in]

where I(**r,s**) is the radiance or the amount of energy that flows across an area at point **r** in the direction of **s.** μ_t is the total attenuation ($\mu_a + \mu_s$) and p(**s**,**s'**) is a probability density function or "phase function" describing scattering in direction **s** for a photon traveling in **s'**. At each point within tissue, energy is lost due to absorption and scattering and gained from energy flow from surrounding areas. The radiative transport

equation, RTE, is difficult to solve and requires constraints on the sample to exactly match assumptions made for an exact solution. The RTE is depicted schematically in Figure 8.

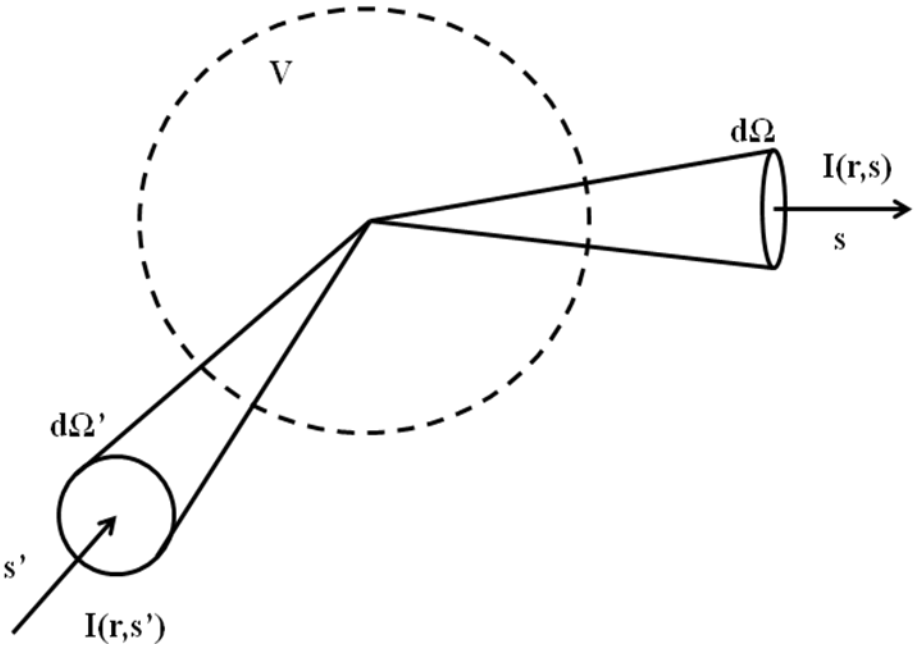

Figure 8: Schematic drawing of energy flow described by the RTE. Within the spherical volume element V, the radiance **I(r,s')** in direction **s'** is either absorbed or scattered in direction **s** within the unit solid angle dΩ.

The IAD method allows for optical property calculations in a wide range of tissue types by approximating a solution to the RTE with an acceptably small error (~3%). IAD calculates the absorption and scattering coefficients using experimentally measured tissue total reflectance and transmission. IAD employs the following steps: 1) guess the optical properties of the tissue (μ_a, μ_s); 2) calculate reflection and transmission

(R_{calc}, T_{calc}); 3) compare calculated values with experimental values; and 4) change guessed μ_a and μ_s until calculated values match experimental values (R_{calc}, T_{calc} = $R_{experimental}$, $T_{experimental}$).

IAD has several advantages and disadvantages[32]. The advantages are that only integrations over angles are required, physical interpretations can be made at each step, and isotropic and anisotropic scattering can be considered. The program is also faster than other methods such as Monte Carlo. Disadvantages are that calculations of internal fluence are awkward and uniform irradiation of optically homogenous slabs is required. Previous studies indicate the disadvantages are minor when measuring skin optical properties making the IAD method appropriate for bulk skin optical measurements[31-33] (See appendix for further discussion of IAD).

An integrating sphere based system is used to measure percent total reflection and transmission (Figure 9)[33]. Integrating spheres convert light into an electrical signal that can be measured by an oscilloscope. Reflectance standards, materials that reflect a known amount of light, are used to calibrate the system for use with actual tissue. Figure 9 shows a simple schematic of a typical experimental setup used to measure transmission and reflection of light in skin.

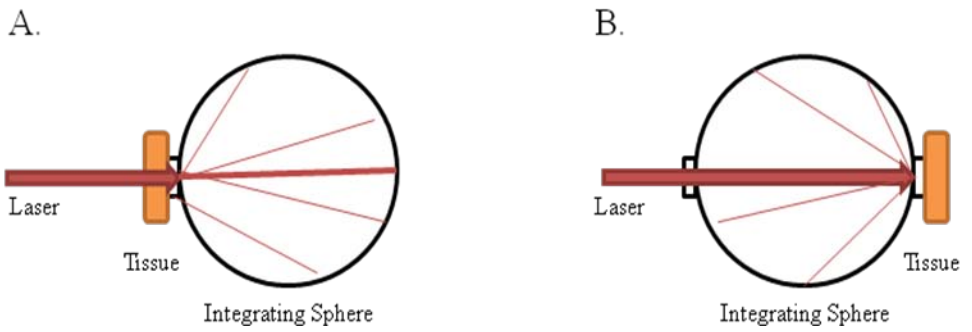

Figure 9: Experimental setup to measure (A) total transmission and (B) total reflectance.

3.2 Controlling the Optical Properties of Skin

3.2.1 Introduction

Traditionally, the optical properties of skin have been considered fixed. However, after tissue immersion in select non-reactive chemical agents, a temporary reduction in light scattering has been demonstrated (Figure 10).

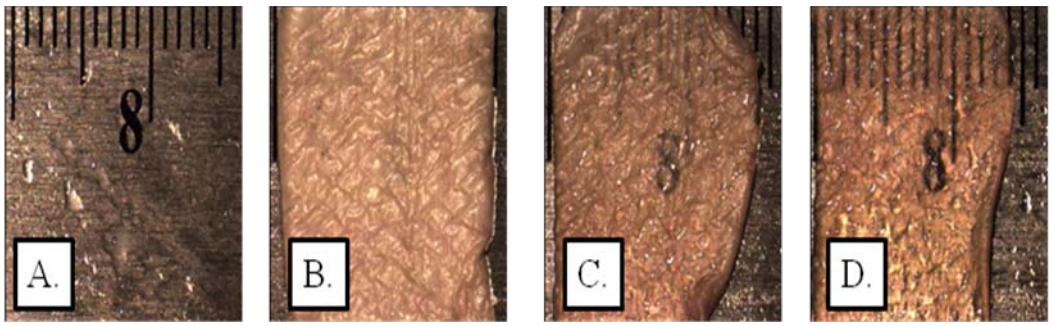

Figure 10: Clearing agents induced transparency in skin: (A) Ruler; (B) Turbid skin on ruler. Reduction of scattering is seen (C) 5 min and (D) 10 min after clearing agent application.

Previous studies have shown that a reduction in tissue optical scattering can improve the efficacy of light based therapeutics[24-34]. Optical clearing can be dramatic as tissue becomes visibly transparent and loses mechanical compliance. This process is reversible when upon subsequent immersion in isotonic saline, tissue turbidity and mechanical properties return to their native states[35]. These clearing agents are benign, biocompatible and already in use as sweetening additives in foods and emollients in skin care products. Optical clearing agents have been investigated primarily in collagenous tissues and have been shown to be most effective when applied directly to the dermis of skin[3-23-28-36-38]. Interestingly, aldehyde fixatives, such as formaldehyde, hinder the clearing process[28]. This section examines changes in optical properties of native and aldehyde fixed skin cleared by a series of sugar-alcohols, propanediols, and sugars (Table 4).

Table 4: Physical properties of clearing agents.

Chemical Agent	Formula	Molecular Weight	Refractive Index	Osmolality (Osm/kg)
Sugar Alcohols:				
Sorbitol	$C_6H_{14}O_6$	182.17	1.45	15.2
Xylitol	$C_5H_{12}O_5$	152.15	1.45	15.6
Glycerol	$C_3H_8O_3$	92.09	1.46	7.60
Ethylene glycol	$C_2H_6O_2$	62.07	1.43	9.00
Propanediols:				
1,2-propanediol	$C_3H_8O_2$	76.1	1.44	8.30
1,3-propanediol	$C_3H_8O_2$	76.1	1.43	8.70
Sugars:				
Sucrose	$C_{12}H_{22}O_{11}$	342.29	1.45-1.50	N/A
Dextrose	$C_6H_{12}O_6$	180.15	1.45	N/A
Fructose	$C_6H_{12}O_6$	180.16	1.45	N/A

3.2.2 Methods of Skin Optical Property Measurement

Ex vivo rodent skin (3-6 wk old Sprague-Dawley) was cut into 1.5x1.5 cm^2 samples using surgical scissors. Subcutaneous fat was removed using a razorblade and rodent skin stored in 1x PBS at 4 ºC until experiments were performed less than 24 hr later. Skin thickness was measured using a micrometer (Mitutoyo, Aurora, IL) after the sample had been placed between two glass slides of known thickness. The slides were secured using binder clips to ensure constant pressure on each skin sample.

An integrating sphere (Labsphere, North Sutton, NH) was used to determine the transmittance and reflectance of 635 nm laser diode light in rodent skin samples[32-33].

The skin/glass combination was placed at the entrance and exit ports of the integrating sphere for transmittance and reflectance measurements, respectively. For transmittance measurements, the exit port was covered using a spectralon-coated port plug (99% reflectance). Light measurements were conducted using a silicon photodiode (Labsphere) connected to an oscilloscope (Tektronix, Beaverton, OR). System calibration was performed using neutral density filters and reflectance standards (Labsphere). The inverse adding-doubling method was used to calculate the reduced scattering coefficient, μ_s', for each skin sample before and after (45 min) clearing agent application. Volume matched solutions of each clearing agent (Table 4) were applied to the dermal side of the skin sample. The chemical agents were applied for a total of 45 minutes and removed carefully with Kimwipes^{TM} prior to transmittance and reflectance measurements. Reduced scattering ratio (RSR) defined as:

$$RSR = \frac{\mu_s'(before)}{\mu_s'(after)} \qquad 3.2$$

the ratio of μ_s' before and after clearing agent application, was used to quantify the reduction in tissue μ_s' and chemical agent optical clearing potential (OCP).

MATLAB software (The Mathworks, Natick, MA) was used to perform a one-way analysis of covariance (ANCOVA) test on the RSR data of rodent skin to test for statistically significant differences in the linear regression for each chemical agent. The overall RSR data were found to be dependent on chemical type (categorical variable) and concentration (continuous variable). The effect of each clearing agent on skin was

assumed to be normally distributed. Analysis by chemical agent with the need to control for the covariate (concentration) called for the use of one-way ANCOVA. An F-test determined that RSR mean values were significantly different and t-tests were performed to compare the effects of the individual chemicals. The Scheffes multiple-comparisons procedure was used to correct for the error associated with the large number of comparisons[39].

3.2.3 Native Skin Clearing

The clearing ability of the agents in Table 4 was examined in native rodent skin and human skin after 45 min of agent application. Figure 11 shows the reduced scattering ratio as a function of clearing agent concentration. The clearing ability of each agent was evaluated from a concentration of 0.1 M to full strength (sorbitol and xylitol up to 7 M; glyercol, 1,2-propanediol, and 1,3-propanediol up to 13.6 M; and ethylene glycol up to 17.8 M). High RSR values indicate a large reduction in scattering within skin. The slope from linear regression analysis was used to define optical clearing potential (OCP) for each chemical agent. Application of one way analysis of covariance to test RSR data identified three significantly different groups ($p \leq 0.05$) among the sugar alcohols and propanediols (Figure 11). Sorbitol was the most effective clearing agent with two fold greater clearing than xylitol, glycerol, and 1,3-propanediol. Ethylene glycol and 1,2-propanediol exhibited the least effective ability to clear.

Clearing in human skin showed similar trends of clearing as those found in rodent skin (Figure 11). Clearing was slightly greater in human skin than rodent,

however, three significantly different groups were seen: sorbitol; glycerol and 1,3-propanediol; and ethylene glycol and 1,2-propanediol ($p \leq 0.05$). Xylitol was not found to be significantly different than sorbitol in human skin. Similar statistical trends in clearing efficacy between rodent and human signify rodent skin as a good experimental model for optical clearing in human skin.

The ability of sugar alcohols and propanediols to reduce light scattering within native skin after 45 minutes of clearing does not correlate with index of refraction or osmolality. Figure 12 illustrates clearing (RSR) in relation to agent osmolality and refractive index. Dehydration (osmolality) and refractive index did not correlate with each agent's ability to clear rodent skin. For example sorbitol and xylitol have similar refractive indices (1.45) and osmolalities (15.2, 15.6 respectively) yet exhibit statistically different clearing efficacies. Previous studies suggested a clearing mechanism based on index matching and dehydration[1-3-23-24-26]. Chemical agents with high refractive index similar to collagen were thought to dehydrate skin tissue and raise the refractive index of the medium surrounding collagen fibers.

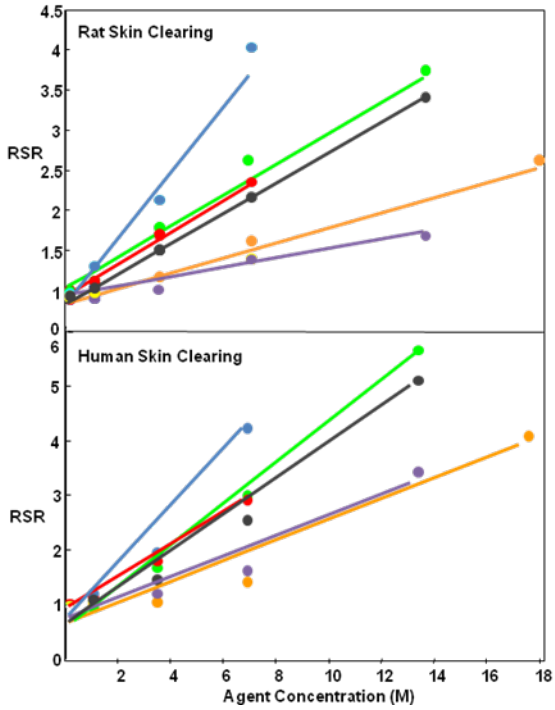

Optical Clearing Potential (slope):

	Rat	Human
Sorbitol	.4060	.5001
1,3-propanediol	.1887	.3221
Glycerol	.1924	.3649
Xylitol	.1987	.2818*
1,2-propanediol	.0892	.1831
Ethylene glycol	.0949	.1826
p-value	≤ .005	≤ .05

Figure 11: Reduced scattering ratio (RSR) of chemical agents in rodent and human skin.

* Xylitol was not found to be significantly different than sorbitol in human skin.

The removal of bulk water from the tissue and subsequent replacement by clearing agent was thought to minimize the refractive index mismatch and reduce scattering. The lack of correlation between refractive index and osmolality with clearing ability cast doubt on these previous assumptions and suggest a more complex molecular mechanism based on clearing agent interaction with collagen.

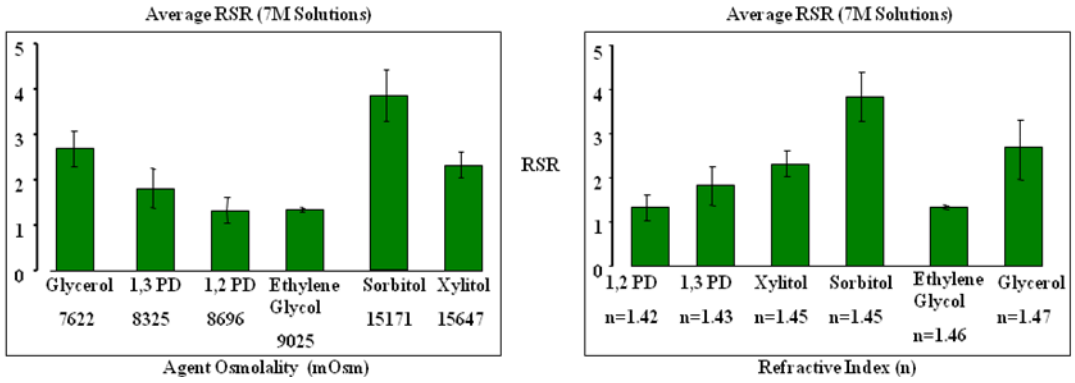

Figure 12: Skin clearing (RSR) does not correlate with osmolality or refractive index.

Optical Clearing in rodent and human skin does correlate with molecular size. Clearing efficacy was proportional to molecular chain length. Sorbitol, a six carbon chain (Mw = 182.17), was the largest sugar alcohol examined and was found to be the most effective clearing agent. Ethylene glycol and 1,2-propanediol were the smallest chemical agents tested and the least effective clearing agents after 45 min.

Hydroxyl group placement also affects an agent's ability to clear skin. 1,3-propanediol and 1,2-propanediol are both similar in size and other physical properties such as refractive index and osmolality. 1,3-propanediol was found to be a significantly more effective clearing agent than 1,2-propanediol after 45 min. 1,3-propanediol has hydroxyl groups on its terminal carbons whereas 1,2-propanediol has hydroxyl groups on adjacent carbons (Figure 13). As we will see later, the longer spacing of 1,3-propanediol's hydroxyl groups allow for a larger interaction with collagen and more effective clearing of skin tissue as a whole.

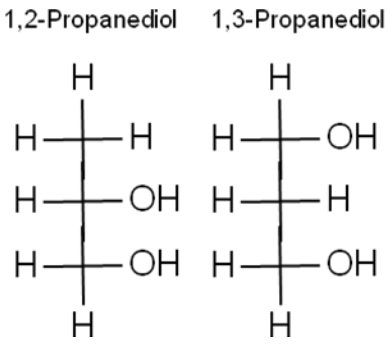

Figure 13: (OH) spacing is larger in 1,3-propanediol leading to more effective clearing after 45 min in native skin.

The ability of a series of sugars to reduce the turbidity of native skin after 45 min of clearing was also examined. Figure 14 shows RSR as a function of clearing agent concentration. Linear regression analysis was again used to determine OCP. Statistical ANCOVA analysis determined a significant difference between glycerol and the other agents indicated by the division in the OCP chart. Like sugar alcohols and propanediols, large sugar molecules are effective clearing agents. Fructose and dextrose, both six carbon molecules, reduce light scattering with no statistical difference compared to the six carbon sugar alcohol, sorbitol ($p \leq 0.05$). The trend of increasing molecular size leading to larger reduction in scattering (high RSR) was found to reach a limit. Sucrose is disaccharide sugar consisting of one fructose and one dextrose molecule. Sucrose was found to have a similar clearing ability to the other sugars. We hypothesize that sucrose's large molecular size sterically hindered its ability to interact with collagen fibers within the skin and limited overall clearing.

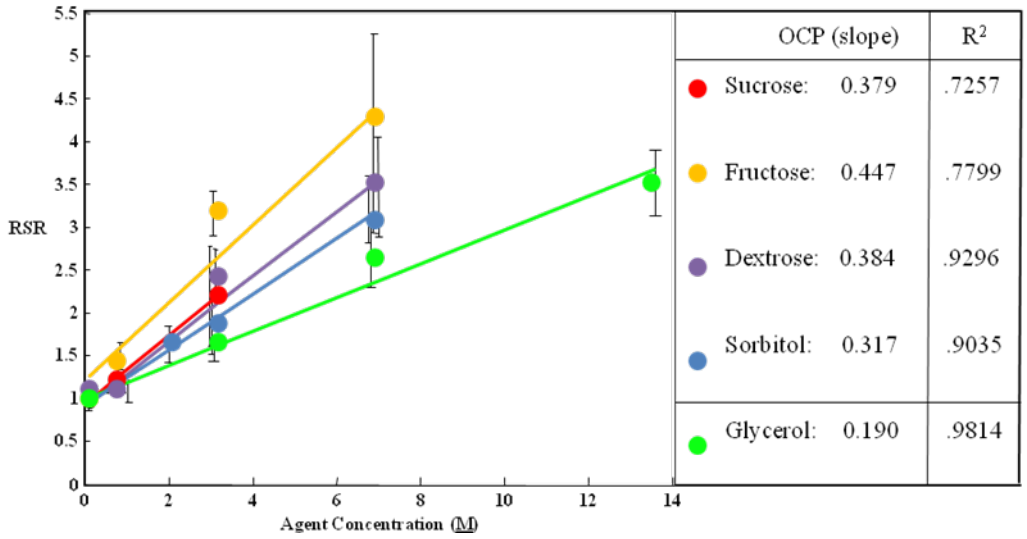

Figure 14: Reduced scattering ratio (RSR) as a function of agent concentration. Optical clearing potential (OCP) of each agent is defined by slope from linear regression analysis of RSR data and shown in inset table.

Clearing in native skin after 45 minutes reveals significant differences in the ability of chemical agents to reduce light scattering. Index of refraction and osmolality are not predictive chemical properties of optical clearing potential. These findings suggest that clearing is more complex than matching an agent's refractive index to the reported values for collagen or simply removing water from skin tissue. Differences in clearing ability cannot be explained by simple diffusion either. Large molecules diffuse more slowly than small molecules throughout tissue, yet they clear more effectively.

The clearing results imply clearing agent interactions with collagen potentially play a large role in optical clearing. Yeh et al, found clearing agents perturb collagen structure in cleared tissues[28]. It was suggested that clearing agents reduce the attractive forces between collagen triple helices which results in collagen structural

changes that lead to clearing. To elucidate the role alterations in collagen morphology play in skin optical clearing, rodent skin tissue was fixed prior to clearing by exogenous chemical agents.

3.2.4 Clearing in Fixed Skin

Fixed tissues exhibit a reduced ability to be cleared leading researchers to suggest collagen structural changes as a possible mechanism for optical clearing. Clearing agents cannot overcome covalent bonds. Fixing tissue introduces an abundance of covalent bonding within skin effectively locking the structure in its native state. A clearing mechanism based solely on collagen perturbation would result in little to no clearing seen in fixed skin immersed in clearing agents.

Excised rodent skin was fixed in 4.0% glutaraldehyde for 48 hr. After fixation, a series of sugar alcohols and propanediols were applied to the skin for 24 hr. The reduction in tissue scattering due to the agents was measured using the integrating sphere technique described above. The reduced scattering ratio (RSR) was calculated and is shown in figure 15 with corresponding standard deviation (Table 5). OCP was calculated for statistical analysis of clearing efficacy, but is not shown.

Given time, clearing agents reduce light scattering within fixed skin. After 24 hr of clearing agent application, scatter reduction in fixed skin was similar to clearing in native skin. Interestingly, there were no differences in clearing ability between the clearing agents examined ($p \leq 0.05$) and each reduced light scattering in fixed skin similar to the most effective agents (sorbitol and sugars) found in native skin after 45 min.

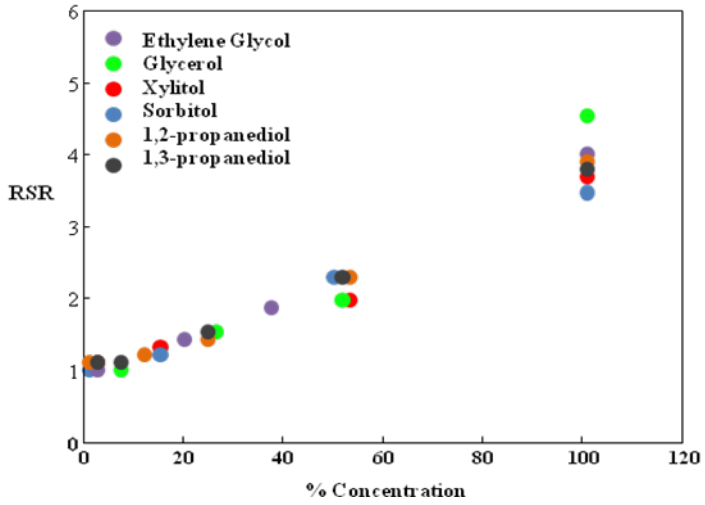

Figure 15: Clearing of rodent skin fixed with 4.0% glutaraldehyde for 48 hr.

Table 5: RSR standard deviation (n=4 at each concentration).

	0.1 M	1.0 M	3.5 M	7.0 M	13.6 M	17.9 M
Ethylene glycol	0.039	0.077	0.256	0.355	N/A	0.425
Glycerol	0.088	0.095	0.227	0.161	0.703	N/A
Xylitol	0.054	0.166	0.299	0.569	N/A	N/A
Sorbitol	0.115	0.001	0.482	0.182	N/A	N/A
1,2-propanediol	0.979	0.151	0.093	0.278	1.33	N/A
1,3-propanediol	0.452	0.082	0.486	0.289	0.986	N/A

Clearing agent ability to reduce scattering in fixed skin indicates that collagen structure perturbation is not the primary cause of scatter reduction. Underlying this result is the assumption that fixatives form covalent bonds throughout the entirety of the collagen fibers. Supporting this assumption are previous studies of glutaraldehyde diffusion through skin that found diffusion of fixative throughout the majority of collagen fibers[40-43]. Cheung et al conducted a comprehensive examination of GA

induced covalent bonding in proteins and collagen fiber networks within pericardium. Glutaraldehyde, a dialdehyde, was found to form intra- and inter-fiber covalent crosslinks between the lysine and hydroxylysine residues of collagen and the aldehyde groups of GA[42].

Initially, it was hypothesized that glutaraldehyde formed polymer networks that quickly crosslinked the surface of collagen fibers limiting the diffusion of the fixative into the interior of the fiber[42]. Recently, however, many studies using Raman, thermal stability, AFM, and enzymatic stability methods have found that an average of three GA molecules bind at each lysine/hydroxylysine residue[40-41-43-44]. These findings, make the early hypothesis of GA polymerization, limiting diffusion into fibrils, seem unlikely[44].

Glutaraldehyde seems to be able to penetrate into collagen fibrils forming crosslinks between triple helices. Cheung found that after fixation with 1% GA, solubilization of collagen within pericardium using CNBr and Pronase was ineffective[42]. Olde Damink found that 85% of free amine groups within 0.5% GA fixed dermal sheep collagen formed Schiff bases which lead to covalent crosslinks[44]. These results indicate a large amount of crosslinking within collagen fibers and fibrils which supports the assumption that native collagen structure is retained throught the clearing process in fixed skin.

3.2.5 Thermodynamics and Kinetics

Clearing experiments in bulk skin tissue point to important processes in the clearing mechanism involving the thermodynamics and kinetics of light scatter reduction. First, there is a thermodynamic equilibrium that is reached between clearing agents and skin. Concentration gradients drive clearing agents to diffuse into skin and remove water. The introduction of clearing agents into the tissue begin to optically homogenize skin and reduce light scatter. Secondly, there is kinetic component to clearing. The speed of clearing differs depending on the clearing agent used and differences between native and fixed skin.

An example of the roles thermodynamic equilibrium and kinetics play in clearing is shown in figure 16. RSR of excised, native rodent skin immersed in 1,2-propanediol and 1,3-propanediol was measured after 1 hr and 24 hr. The optical clearing potential, OCP, was calculated as described above. After 1 hr of clearing there was a significant difference in clearing ability. 1,3-propanediol was found to clear more effectively than 1,2-propanediol. After 24 hr of clearing, however, there was no difference ($p \leq 0.05$). 1,2-propanediol and 1,3-propanediol have similar refractive indices and osmolalities. They differ in hydroxyl group placement and ability to hydrogen bond with collagen. 1,3-propanediol's greater collagen affinity allowed for faster clearing in rodent skin and suggests a clearing mechanism based on clearing agent interaction with collagen.

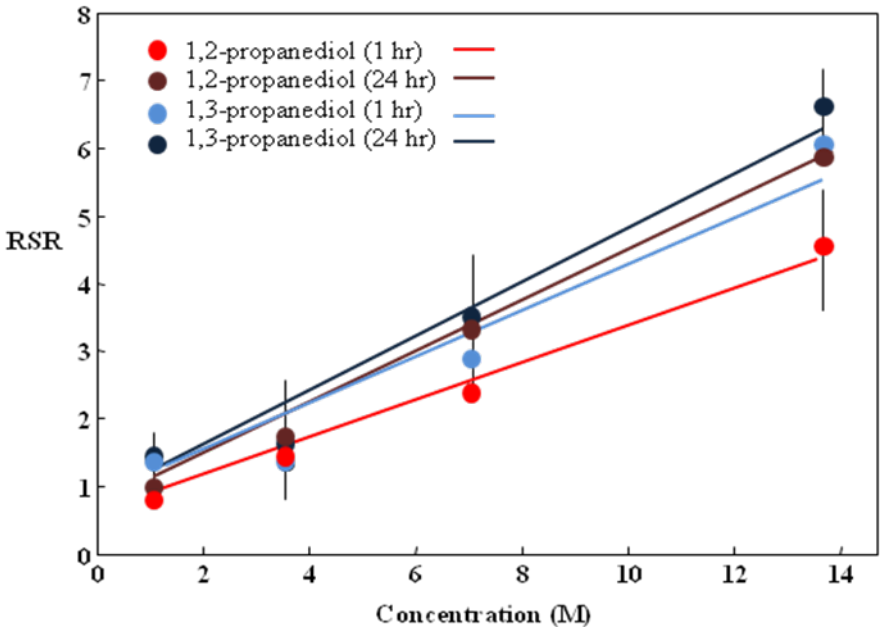

Figure 16: Reduced scattering ratio (RSR) as a function of agent concentration in native rodent skin after 1 and 24 hours. Linear regression lines indicate optical clearing potential (OCP). Non-visible error bars indicate standard deviation smaller than data point.

Ultimately all clearing agents studied with high refractive indices and osmolality eventually clear skin given sufficient time. The speed of clearing is dependent on the collagen affinity of the agent used. Light scatter reduction depends on optically homogenizing skin by reducing refractive index mismatches within the tissue. As seen in the following sections, optically homogenizing skin requires clearing agent diffusion through collagen fibers with removal of tightly held bound water.

CHAPTER IV

MOLECULAR MODELING OF CLEARING AGENT INTERACTION WITH COLLAGEN

Molecular dynamics simulation is an ideal tool to probe molecular level phenomenon, as it provides atomic level insight to enhance qualitative understanding of molecular interactions. Briefly, molecular dynamics is based on Newton's second law of motion. Force on each atom is computed using a force field and the system of equations is integrated to get the time evolution of positions, accelerations, and velocities of atoms. The force field, or potential field, includes bonded (harmonic bond length, bond angle, and torsional) and non-bonded (Vanderwaal's and electrostatic) energy terms as a function of the position of atoms which can be used to compute atomic forces[45].

CHARMM molecular dynamics package with param22 force field in implicit solvent conditions was used to probe the interaction of alcohols with collagen mimetic peptides[46-47]. Collagen mimetic peptides are short triple helical domains like collagen having few (typically 7-12) amino acids in each alpha chain.

Note: Molecular dynamics simulation performed in collaboration with Krishnakumar M. Ravikumar and Professor Wonmuk Hwang.

These synthetic peptides have provided useful insights into the structure, function, and their relationship in collagen and are useful for simulation studies owing to their smaller size[48].

4.1 Structure of Peptides and Alcohols

Small modeling peptides are commonly used to quickly and accurately model collagen. Synthetic peptides 1BKV (Protein Data Bank ID) and a regular GPO peptide, $((GPO)_{10})_3$ (G-Glycine,P-Proline, and O-Hydroxyproline), were used in the simulations. Peptide 1BKV has a biologically relevant imino acid deficient sequence of type-III collagen, which is important in its cleavage[48-49]. Peptide GPO is an imino acid rich peptide whose backbone structure was built using the TheBuSr collagen building script[50]. The side chain atoms were added to the backbone using the existing amino acid topology files and systematically energy minimized as reported previously[49] to get the final structure. Polar hydrogens were added to the peptides using the HBUILD facility in CHARMM[51]. Parameters for hydroxyproline were added from a previous study[52]. Structures of the 6 alcohols - ethylene glycol, glycerol, 1,2-propanediol, 1,3-propanediol, xyletol, and sorbitol were built from the already existing lipid topology and parameter files.

4.2 Simulation Setup

Each alcohol was simulated with both peptides making a total of 12 separate simulation runs. In each simulation, 20 alcohol molecules were placed randomly around the peptide at a radial distance of 12.0 Angstroms from the cylindrical axis of the peptide. Owing to their bigger molecular structure, only 12 molecules of xylitol and sorbitol were placed around the peptide. Generalized Born solvation energy with simple smoothing function at the dielectric boundary was used to mimic solvation effects[53]. The systems were first energy minimized to remove close contacts and then heated at the rate of 5 K/ps for 60 ps to get to the desired temperature of 300 K. The systems were then equilibrated for 40 ps at 300 K. Each production run was for 600 ps using Verlet integration algorithm with a time step of 2.0 fs; coordinates were saved every 1 ps. To prevent the diffusion of peptide, harmonic constraints (spring constant = 2 kCal/mol-A) were applied on all peptide atoms to their original positions during heating and equilibration. During the production run, harmonic constraints were applied only on backbone amide nitrogen, alpha carbon, and carboxyllic carbon atoms, leaving the rest of the atoms, including side chains, free to interact with the alcohol molecules. To prevent diffusion of alcohol molecules away from the peptide, a cylindrical potential shell of 40 Angstroms diameter was defined around the peptide. Whenever alcohol molecules attempted to move out of this shell, a harmonic force was applied (spring constant = 1 kCal/mol-Å) pushing the alcohols back into the cylindrical shell.

4.3 Analysis

The hydroxyl groups in alcohols, being donors and acceptors of hydrogen bonds, can interact with the peptide side chains, backbone amide hydrogens, and carboxyllic oxygens. Hydrogen bonding and hydrogen bond bridge formation of sugar alcohols and propanediols were analyzed. Hydrogen bonds were defined using a distance cutoff of 2.4 Å[54] and a bridge was defined to be formed between two alpha chains if an alcohol molecule is simultaneously hydrogen bonded to two alpha chains or two amino acids in the same alpha chain. Bridges can span across the surface area of collagen disrupting ordered water hydration layers. The propensity of chemical agents to form hydrogen bonds and bridges can be considered as a measure of its affinity to the collagen surface and is potentially related to its optical clearing properties.

Table 6: Average number of hydrogen bonds and bridges formed.

Chemical	Hydrogen Bonds (#/ps)	Bridges (#/ps)
Ethylene glycol	0.73430	0.2758
1,2-propanediol	0.75304	0.3174
1,3-propanediol	0.76562	0.3279
Glycerol	0.78600	0.3318
Xylitol	0.78700	0.3525
Sorbitol	1.51854	1.0866

Table 6 shows the series of sugar alcohols and propanediols modeled in this study with the average number of formed hydrogen bonds and bridges per picoseconds of each agent. Ethylene glycol with two hydroxyl groups forms the least number of hydrogen bonds and bridges. The average hydrogen bonds and bridges formed increase with increasing molecular size with sorbitol forming the most number of hydrogen bonds and bridges. Large amounts of formed hydrogen bonds and bridges indicate a high collagen affinity of the agents and an increased ability to displace water and dehydrate collagen. These results correlate with our previous skin clearing experiments and suggest that collagen affinity and dehydration play a fundamental role in reducing the light scattering within tissues. Though we did not include explicit water in our simulations, one expects that the relative hydrogen bonding propensities of sugar alcohol and propanediol molecules to remain the same. Figure 17 shows a CHARMM simulation of 1,3-propanediol (green) penetrating into the groves on the surface of the triple helix shown in blue, red, and gray. Collagen molecules have a dense ordered first hydration shell of water which can be disrupted by clearing agents. Clearing agents like alcohols penetrate into the grooves on the surface of collagen forming hydrogen bonds and bridges with collagen and hydration water. This interaction leads to disruptions in the native water hydration layer around collagen.

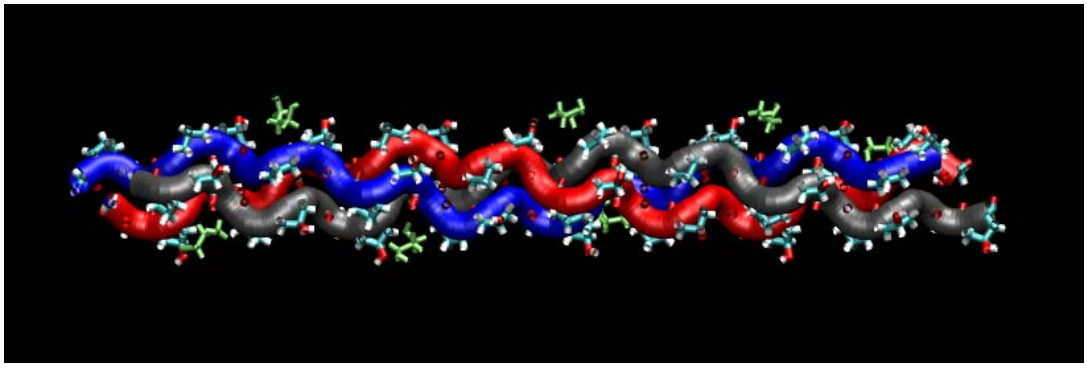

Figure 17: CHARMM model of 1,3-propanediol (green) in the grooves of the collagen triple helix backbone (red, blue, gray). Infiltration of clearing agents such as 1,3-propanediol can disrupt the water hydration structure of collagen.

The number of hydroxyl groups and the position of hydroxyl group can have significant influence in the above process. In this regard, 1,3-propanediol with its hydroxyl groups far apart on terminal carbons might disrupt the native collagen hydration better than 1,2-propanediol, whose hydroxyl groups are much closer to each other on adjacent carbons. Sorbitol's large size with six hydroxyl groups allows the formation of additional hydrogen bonds with collagen. Sorbitol's large collagen affinity leads to an increased disruption of collagen's hydration shell. CHARMM simulations of the clearing agents 1,3-propanediol and sorbitol's interaction with collagen were examined and are illustrated in Figures 18 and 19. Sorbitol's large size allows for the formation of an additional hydrogen bond with collagen. This increase in collagen affinity is exhibited by the marked increase in hydrogen bonding and bridge formation modeled by CHARMM and correlates well with previous findings that sorbitol is an effective clearing agent[55].

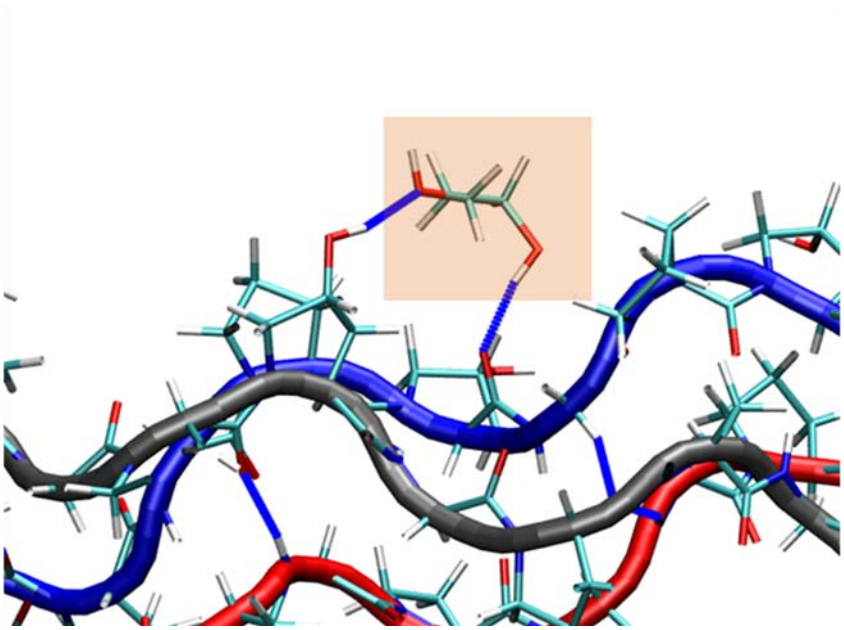

Figure 18: 1,3-propanediol (pink box) forms a bridge between hydroxyproline in one alpha chain (gray) and the backbone (–C=O) group in another alpha chain (blue).

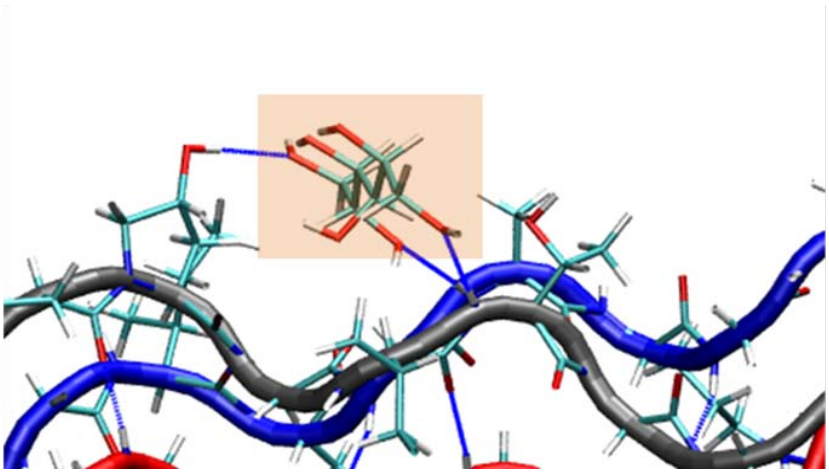

Figure 19: Sorbitol (pink box) forms a bridge between hydroxyproline in one alpha chain (gray) and the backbone (–C=O) groups (2) in another alpha chain (blue). Sorbitol's large size allowed the formation of an additional (third) hydrogen bond with collagen.

Overall the trends found using CHARMM simulations mirrored the results of the bulk skin clearing experiments discussed previously. Large alcohols disrupt the hydration layer more effectively than small molecules due to the increase in hydroxyl groups. The inability of water molecules to displace large clearing agents prevents the hydration layer from reforming. These results suggest hydrogen bonding or bridging leading to collagen dehydration is a key factor responsible for optical clearing. The following chapters investigate the relationship between collagen dehydration and skin optical clearing.

CHAPTER V

CLEARING AGENT INDUCED CHANGES OF COLLAGEN STRUCTURE

5.1 Clearing Agent Interaction with Collagen on the Microscopic Level

Clearing agent interaction with collagen was found in both bulk skin optical property measurements and molecular dynamic modeling to play a fundamental role in optical clearing. Previous studies indicated that clearing agents induce structural changes in the collagen of native skin[28]. Nonlinear optical microscopy was used to investigate collagen structure in native and cleared skin.

5.2 Clearing Agent Activity on Collagen Reduces Tissue Scattering

Nonlinear optical microscopy (NLOM) is a laser scanning technique that can render thin images from within intact, living tissues[56-57]. Nonlinear optical phenomena result from the modification of the optical properties of a material system by the presence of sufficiently intense light[58]. Optical phenomena are considered "nonlinear" when the response of a material system to an applied optical field depends in a nonlinear fashion. The polarization equation, equation 5.1, describes how the dipole moment per unit volume, or polarization **P(t)**, of a material system depends upon an applied optical (electric) field, **E(t)**.

$$P_i(t) = \chi_{ij}^{(1)} E_j(t) + \chi_{ijk}^{(2)} E_j(t) E_k(t) + \cdots \qquad 5.1$$

The constant of proportionality, χ, is a tensor describing the material properties of the medium and is known as the susceptibility. The first term in the polarization equation, $\chi^{(1)}E(t)$, describes linear events such as absorption and scattering. Nonlinear events are described by the higher order terms. Second order interactions such as second harmonic generation (SHG) or frequency doubling, (detailed below) is described by $\chi^{(2)}$, a tensor of the third rank, and two electric fields, E(t)E(t). For a more rigorous derivation of nonlinear events and second harmonic generation please see the appendix.

Endogenous two-photon fluorescence excitation and second harmonic generation (SHG) have been characterized for collagen; SHG can provide a unique spectral signature for collagen specific imaging[56-59-61]. SHG in fibrillar collagen has been used to enhance NLOM image contrast and constituent specific segmentation in skin,[28] cornea[60] and articular cartilage[61] without using exogenous stains or dyes.

Second harmonic generation is a second order, nonlinear interaction where two photons with frequency, ω, incident upon a material interact with the medium to form one photon consisting of twice the original frequency (2ω). SHG is described by the second term in the polarization equation:

$$P^{(2)}(t) = \chi^{(2)}E(t)E(t) = 2\chi^{(2)}EE^{*} + \left(\chi^{(2)}E^{2}e^{-2\omega t} + c.c.\right). \quad 5.2$$

where:

$$E(t) = Ee^{-i\omega t} + c.c. \quad 5.3$$

equation 5.2 dictates that two sources contribute to second order polarization. The first term of equation 5.2 ($2\chi^{(2)}$ EE*) is time independent and forms a static field in the material called optical rectification. The second term is frequency doubled and can lead to the generation of radiation at the second harmonic frequency.

A necessary condition for SHG is that the constituent molecules lack an inversion center. Fibrillar collagens satisfy this condition; its secondary structure is an alpha helix. For type I collagen, two identical α1(I) and one α2(I) chains form a triple helix. Despite 30 years of research, the fine structure and assembly mechanisms of collagen structures remain topics of intense study and inquiry[30-62-64]. High-order, macroscopic collagen structures exhibit long range molecular order, providing a nonlinear medium with characteristic lengths on the order of near-infrared wavelengths. Disruption of long range molecular order extinguishes SHG, making it sensitive to perturbations of collagen structure and useful for optically monitoring denaturation[65-67].

NLOM was used previously to image collagen with SHG in tissues during optical clearing and subsequent rehydration after applying glycerol and saline, respectively[28]. Tissue systems investigated were fibroblast-seeded collagen tissue constructs and rodent skin, both untreated and fixed. For fibroblast-seeded collagen tissues, application of glycerol resulted in loss of SHG from collagen and concomitant increase in gel transparency. Loss of SHG was indicative of collagen destabilization by glycerol, an effect demonstrated with electron[68] and polarization light microscopy[28] in glycerinated rodent tail tendon. Application of glycerol to rodent skin did not

extinguish SHG signal, but fibrous collagen morphology unraveled to a matted appearance concomitant with increased tissue transparency.

Subsequent rehydration with saline in fibroblast-seeded collagen tissues restored SHG signal, fibrous collagen morphology and gel turbidity. Similarly, rehydration of rodent skin with saline resulted in reformation of fibrous collagen morphology and return in tissue turbidity. Differences observed by NLOM in optical clearing of fibroblast-seeded collagen tissue and rodent skin were hypothesized to be due to the presence of native covalent cross-links. Indeed, formalin fixation of these tissues limit glycerol induced optical clearing and morphological changes to collagen as measured by NLOM.

An example of SHG images of collagen in native and fixed rodent skin after clearing is shown in figure 20. Collagen in its native state has a ribbon-like morphology characteristic of large fibers. Native and fixed rodent skin was submerged in clearing agents and imaged using second harmonic generation after 1 hr and 24 hr respectively. Clearing agents induce structural changes in native collagen after 1 hr (left column figure 20). Interestingly the magnitude of dissociation appears to correlate with clearing efficacy. Larger agents such as xylitol, sorbitol, and high fructose corn syrup (90% fructose) induced large changes in collagen structure. Smaller agents such as 1,2-propanediol only minimally perturbed collagen structure.

Native collagen structure is retained after clearing in fixed skin (figure 20 right columns). Glutaraldehyde produces an abundance of covalent crosslinks between collagen triple helices that clearing agents are unable to overcome. This result is not

surprising and is in agreement with our previous finding that clearing is not dependant on collagen structural changes.

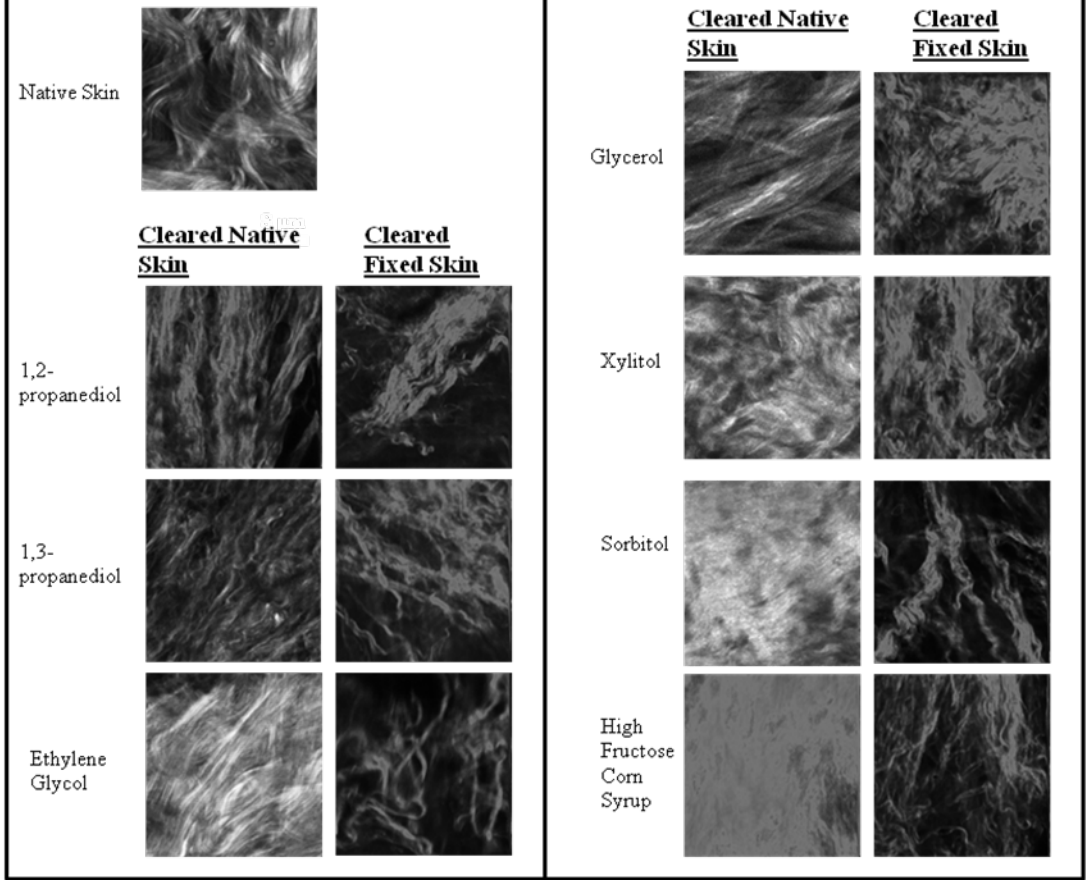

Figure 20: SHG images of collagen in native and fixed rodent skin after clearing for a series of clearing agents. Collagen structure is perturbed in native skin while the ribbon-like structure is retained in fixed skin. Images are 84x92 μm.

Clearing agent induced changes in collagen structure correlate with clearing efficacy. In chapter III we showed that larger chemical agents clear native skin more

effectively than smaller agents. As a result the collagen structure is perturbed. These findings support modeling results in chapter IV. Clearing agents diffuse into collagen fibers, remove water, resulting in marked changes of fiber morphology. In contrast, fixed tissues exhibit a reduced clearing efficacy. We will examine this phenomenon more closely in the following chapters.

CHAPTER VI

COLLAGEN FIBRILLOGENESIS INHIBITION AND SOLUBILITY

6.1 Destabilizing Effect of Glycerol on Collagen in Rodent Tail Tendon

Destabilization of native collagen structures using non-reactive chemical agents is a surprising finding. Type I collagen is the predominant structural component in most biological tissues and shows increased thermal stability against denaturation in solution with sugar-alcohols[69-71]. The earliest evidence of native collagen dissociation using glycerol was reported over 20 years ago using transmission electron microscopy (TEM) and x-ray diffraction (XRD) techniques to measure collagen fiber structure in rodent tail tendon following one of six exposures: 1) water, 2) phosphate buffer, 3) glutaraldehyde, 4) glutaraldehyde followed by glycerol, 5) glycerol, or 6) glycerol followed by phosphate buffer[68]. Consistent with results observed using NLOM[28], only glycerol treatment induced swelling of interfibrillar space, dissociation of collagen fibrils into microfibrils (and loss of characteristic banding in some regions) as observed using TEM and molecular disorder as measured with XRD. Ultrastructurally, glutaraldehyde fixation (exposure 4) reduced the dissociative effects whereas rehydration with phosphate buffer (exposure 6) reversed the dissociative effects of glycerol[68]. These ultrastructural and NLOM studies show that: 1) bonding forces for high order collagen structures are primarily non-covalent in nature; 2) glycerol interrupts these bonding forces; and 3) upon rehydration, these bonding forces are restored as evidenced by reassembly of high order collagen structures.

6.2 Molecular Interactions of Agents with Collagen *in vitro*

Studies using synthetic collagen-like peptides show that stable formation of secondary, tertiary and, consequently, higher order structures depend on specific binding sites[72]. Stability of secondary and tertiary structures is enhanced by inductive (electronegativity) effects provided by hydroxylated proline residues[73]. For quaternary and higher order structures, attractive forces mediated by hydrophilic environments[74] are preeminent, and sugars and sugar-alcohols can be used effectively to elucidate collagen interactions and self-assembly mechanisms.

6.2.1 Hydrogen Bonding in Fibrillogenesis

The dynamics of collagen fibril formation can be described by nucleation followed by growth during which higher order structures (fibrils) develop[29]. Non-covalent forces driving collagen fibrillogenesis could include, for example, hydrogen bonding, van der Waals and steric interactions. Sugars and sugar-alcohols have been used to modulate and characterize these forces[29-75-79] in conjunction with measurement techniques utilizing osmotic pressure to study macromolecular interactions[80]. Typically, these techniques apply force through osmotic pressure via polymer solutions and measure intermolecular distance by XRD. Force-distance measurements have been performed using concentrated collagen thin films immersed in solutions of polyethylene glycol (PEG)[75-78-80]. PEG does not penetrate these thin films, thus exerting osmotic pressure on the collagen fibers in a manner directly related to its concentration. Osmotic removal of water decreases the molecular separation of

triple helices; this osmotic force is balanced by repulsion. Decreasing PEG concentration corresponded with decreasing osmotic pressure and increasing interaxial distances until attractive forces dominated. These attractive forces are responsible for molecular recognition and drive collagen fibrillogenesis.

Collagen attractive forces may be characterized with the addition of sugars and sugar-alcohols. These agents screen collagen attractive forces resulting in force-distance measurement curves that reflect intermolecular repulsion. Collagen attractive forces were characterized by taking the difference between curves, with and without agents, as a function of interaxial distance[75-78].

Force-distance measurements of collagen led to two significant findings in determining the mechanism for fibrillogenesis: 1) the repulsive force increases exponentially with a decrease in interaxial spacing (1.5 - 2.0 nm); and 2) both interhelical spacing and net repulsive force decrease with an increase in temperature[77]. These findings, along with the discovery that force-decay lengths and force magnitudes are insensitive to ionic strength at high osmotic stress, suggest that either "hydration forces" between polar surfaces or the "hydrophobic effect" of nonpolar moieties is the dominant force in fibrillogenesis. Although the temperature sensitivity of attraction is qualitatively consistent with both hydration forces and the hydrophobic effect, the magnitude of this sensitivity suggests a hydrophilic mechanism[78].

A mechanism for fibrillogenesis was further defined when considering the effects of pH on collagen fiber formation. Collagen fibrillogenesis was strongly favored at physiologic pH (~7.4). However, when pH was lowered to 6, there was substantial

weakening of the attraction between collagen helices – consistent with titration of specific hydrophilic residues[78]. pH effects suggest involvement of histidine residues which have the lowest pK_a value of the three basic amino acids making it the most sensitive to reduction of pH from 7.4 to 6. At neutral pH, histidine is neutral and forms hydrogen bonds as a proton acceptor. Reducing pH protonates histidine whereby it becomes a hydrogen bond donor and disrupts the interactions between helices. The reaction of collagen to pH, in conjunction with force-distance measurements, support hydrophilic interactions as the main driving force for fibrillogenesis.(26, 59, 61, 62)

6.2.2 Collagen Solubility (Inhibition of Fibrillogenesis)

Collagen solubility refers to soluble collagen remaining in solution after fibrillogenesis. Addition of sugars and sugar-alcohols in previous studies were shown to enhance collagen solubility in buffered saline by masking hydration mediated attractive forces between helices and inhibiting fibrillogenesis[29-71-75-79]. These chemical agents slow and limit fibrillogenesis by disrupting hydrogen bond facilitated water bridges between collagen helices. The efficiency of fibrillogenesis in the presence of glucose, fructose and sucrose (figure 21) as well as ethylene glycol, glycerol and sorbitol (figure 21) has been studied previously and showed an inverse dependence on agent chain length[29-75]. Ethylene glycol was the shortest (two carbon chain) agent tested and displayed little effect on collagen fibrillogenesis and solubility[75]. Inhibitory effects of glycerol on collagen self-assembly are well documented[29-75-79]. Sorbitol is twice as long as glycerol (6 and 3 carbons, respectively) and has twice the collagen

solubility[75]. Glucose and fructose are six carbon sugars and show greatest collagen solubility when compared to sugar-alcohols (ethylene glycol, glycerol and sorbitol) [75]. Sucrose, a disaccharide of glucose and fructose, showed similar inhibitory effects on collagen fibrillogenesis as with the monosaccharides[29].

Insight into the difference in collagen solubility between ethylene glycol and glycerol can be gained by comparison studies of 1,2- and 1,3-propanediol which both have similar dielectric properties, e.g., their indices of refraction are 1.43 and 1.44, respectively. If electrostatic, van der Waals, or hydrophobic interactions were the major attractive forces in fibrillogenesis, these two agents should have similar collagen solubilities. In fact, 1,3-propanediol had ~20 times greater collagen solubility (comparable with glycerol) than 1,2-propanediol which showed comparable collagen solubility with ethylene glycol[75].

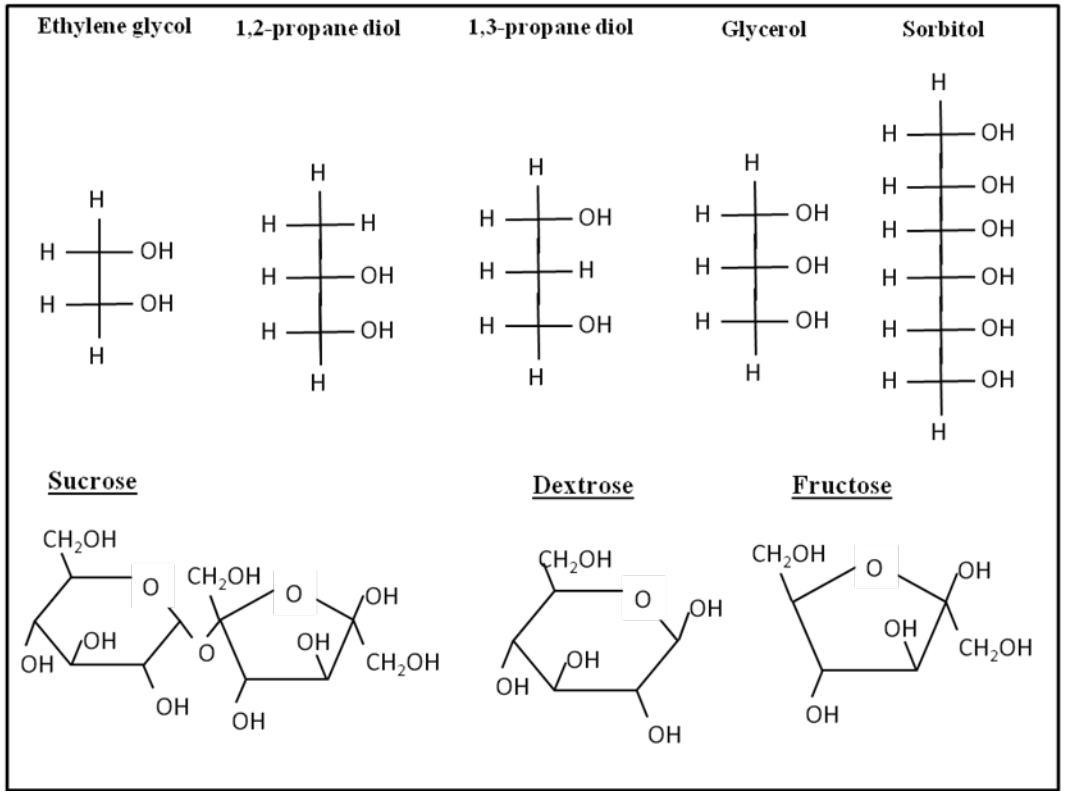

Figure 21: Molecular structures of sugar alcohols and sugars.

Collagen solubility of propanediols and ethylene glycol, glycerol and sorbitol suggests a stereochemical effect[75-78]. For propanediols, adjacent or terminal placement of hydroxyl groups on the three carbon backbone has dramatic effects on collagen solubility. This is reflected in sugar-alcohols where ethylene glycol (glycerol) and 1,2- (1,3-) propanediol have similar distances between hydroxyl end groups. Placement of hydroxyl end groups on 1,3-propanediol and glycerol may correspond to the spacing of hydrophilic interaction sites of collagen tertiary structures. The fact that sorbitol has twice the collagen solubility as glycerol is supportive, but studies with sugar-alcohols of other chain lengths would further refine this hypothesis.

6.2.3 Expanded Collagen Solubility Study

Collagen fibrillogenesis inhibition and solubility for a series of chemical agents were examined to corroborate and expand previous studies and to evaluate these properties as possible predictors of clearing efficacy. To date, selection of potential agents has been empirical rather than based upon fundamental understanding of chemical agent induced tissue optical clearing. Common properties of optical clearing agents such as sugars and sugar-alcohols have suggested refractive index matching with native tissue components, in particular collagen, and dehydration as possible mechanisms of tissue optical clearing[2-24]. Under this proposed mechanism, refractive index matching of the clearing agent to that of collagen would reduce light scattering leading to an increase in tissue transparency. Dehydration was also believed to play a role as reported chemical agents are hyperosmotic with respect to tissue. However, use of these properties as selection criteria does not predict agent optical clearing potential (OCP) [27-81] which suggests an incomplete understanding of chemical induced tissue transparency.

Previous studies have suggested molecular interactions of chemical agents with collagen have a prominent role in tissue optical clearing[82]. It has been shown at microscopic and ultrastructural length scales that glycerol, a prototypical optical clearing agent, destabilizes high-order collagen structures and that this is an effect of agent induced tissue transparency[28-68]. In addition, glycerol's non-reactivity with collagen facilitates reversibility of its optical clearing effects. Attractive forces between collagen triple helices drive collagen fibrillogenesis from solution and have been characterized in

the presence of sugars and sugar-alcohols[75]. Here we introduce collagen solubility as a measure of a chemical agent's ability to screen non-covalent forces and correlated it with tissue optical clearing for a series of polyols.

In vitro self-assembly of solubilized (pH ~ 3) rodent tail collagen I (BD Biosciences) into fibrils was carried out in phosphate buffered saline (PBS) (0.138 M NaCl, 0.0027 M KCl). Stock collagen solutions (4.26 and 4.27 mg/ml) were diluted to concentrations of 0.25, 0.75, 1.50, and 2.13 mg/ml. These solutions were mixed with chemical agents of various concentrations. Ethylene glycol, glycerol, xylitol, sorbitol, 1,2-propanediol, 1,3-propanediol, dextrose, fructose, and sucrose (Sigma Aldrich) were all reagent grade quality and used without further purification. With addition of NaOH, the solutions were adjusted to physiological pH (~ 7.4), inducing collagen fibrillogenesis, and incubated at 37º C for 24 hours. After fibrillogenesis was complete, the solutions were centrifuged at 12,000 rpm for 15 minutes to separate fibrils (white precipitate) from the remaining collagen molecules (supernatant). Collagen solubility was measured by optical absorbance of the supernatant (Figure 22). See appendix for more detailed discussion on optical absorbance and spectrophotometry. Collagen concentration is commonly measured optically using peaks at 215-230 nm and 276 nm. A calibration curve was determined by measuring optical absorbance at 215-230 nm and 276 nm[83] (USB2000, Ocean Optics) of a series of known collagen solutions at different concentrations. Optical absorbance at 215-230 nm and 276 nm was used to measure collagen concentration in solution. Measured collagen concentrations using

absorbance were consistent with each other when comparing a minimum of three samples at each agent concentration.

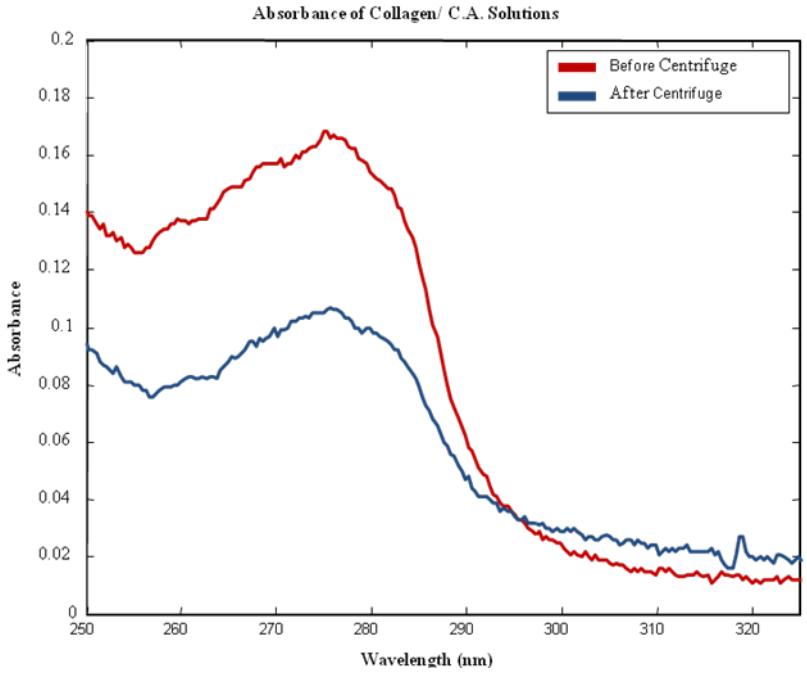

Figure 22: Soluble collagen absorption peak (276 nm) before (red) and after (blue) fibrillogenesis.

Estimated fibril formation is shown in Figure 23 for 1.4 M chemical agent concentration. Straight lines are guides to the eye and calculated by linear regression. Fibrillogenesis inhibition manifests in two ways. First, there is a reduction in regression line slope indicative of a lower formation efficiency. Second, the x-axis intercept is increased resulting in higher concentrations of collagen being needed for fibrillogenesis to occur. Ethylene glycol and 1,2-propanediol showed negligible inhibitory effects on

collagen fibrillogenesis. With these agents, efficiency of fibril formation was near unity, mirroring collagen self-assembly in PBS (not shown). Longer chain polyols such as glycerol, xylitol, sorbitol, and 1,3-propanediol showed increasing chemical agent concentration, consistent with previously reported results[75-79].

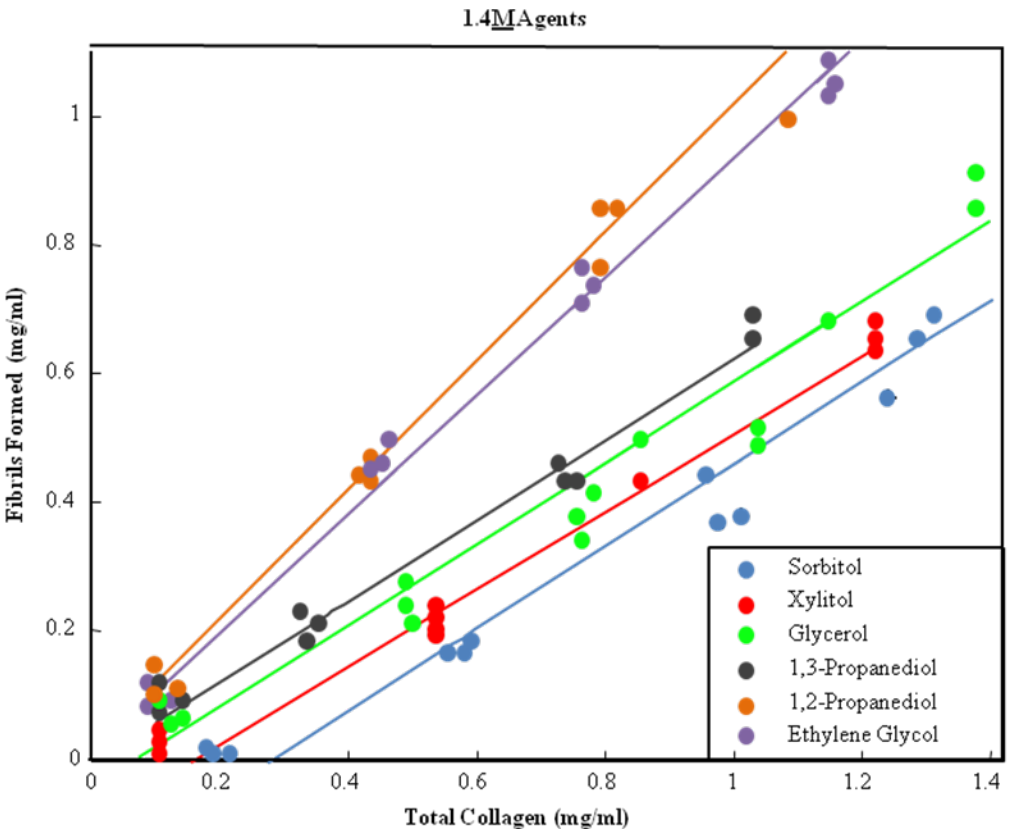

Figure 23: Collagen fibril formation. Fibrils formed from total collagen in 1.4 M solutions of each chemical agent.

Collagen solubility as a function of chemical agent concentration is shown in figure 24. Solubility is quantified as the amount of collagen remaining in supernatant following fibrillogenesis. In this data set, the initial collagen concentration was 1.25

mg/ml. As would be expected from the data shown in Figure 23, ethylene glycol and 1,2-propanediol showed low collagen solubilities. With glycerol, 1,3-propanediol, xylitol, and sorbitol solutions, their collagen solubilities increased with increasing chemical agent concentration. Sorbitol exhibited twice the collagen solubility of glycerol and 1,3-propanediol, consistent with previously reported results[75]. Overall the data demonstrated an increase in collagen solubility with increasing sugar alcohol chain length from ethylene glycol (2 carbon chain) to sorbitol (6 carbon chain).

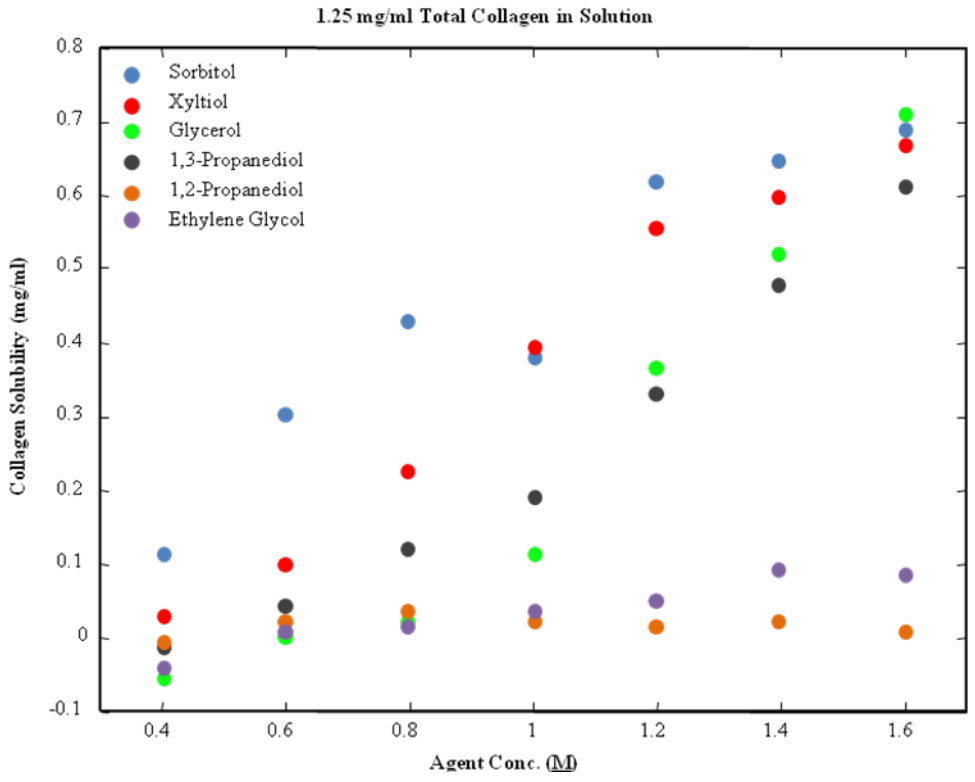

Figure 24: Collagen solubility of sugar alcohols and propanediols. Quantity of collagen remaining in solution as a function of chemical agent concentration.

Collagen fibrillogenesis and solubility for a series of sugars were also examined. Fibril formation from 0.4 M solutions of chemical agents is shown in figure 25. For collagen in PBS only, fibrillogenesis efficiency is near unity and depicted by the bold black line. Sugars showed higher fibrillogenesis inhibition than sugar alcohols or propanediols. Sucrose was the largest molecule tested and had the greatest inhibiting effect on fibrillogenesis. Fructose, dextrose, sorbitol, and glycerol showed decreasing inhibition of collagen fibrillogenesis.

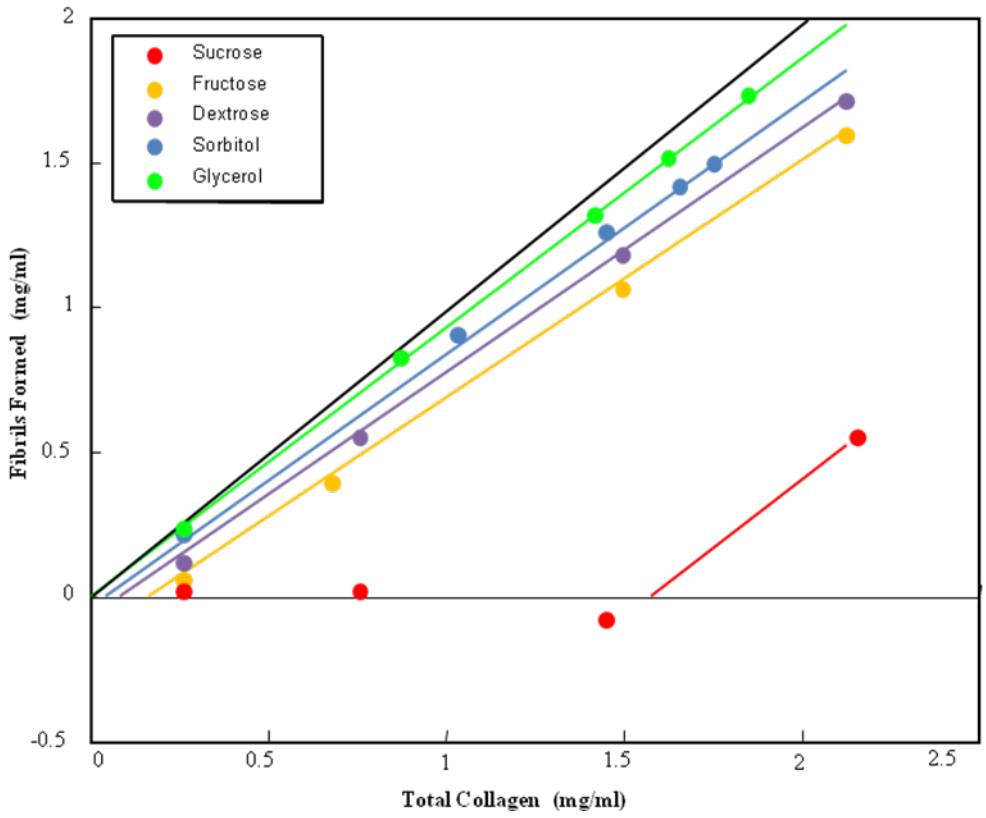

Figure 25: Collagen fibrils formed for sugars and sugar alcohols. All agents shown have a concentration of 0.4 M.

Collagen solubility for the series of sugars is shown in figure 26. The previous study found that solubility increased with increasing sugar alcohol chain length. The sugars continued this trend with sucrose having the highest collagen solubility followed by fructose, dextrose, sorbitol, and glycerol.

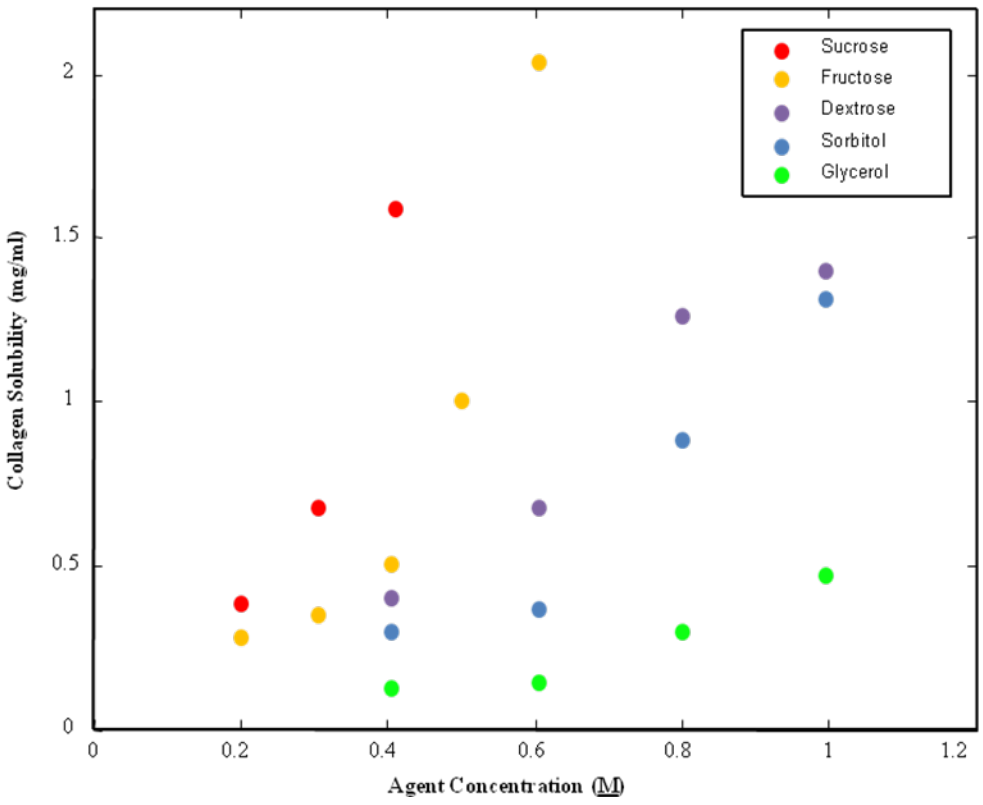

Figure 26: Collagen solubility as a function of agent concentration for a series of sugars and sugar alcohols.

Chemical agents that can induce tissue optical clearing solubilize collagen by suppressing hydrophilic, intermolecular interactions. The propanediols evaluated have been used previously to highlight the role of hydrogen bonding in collagen

fibrillogenesis[75]. Suppression of these hydrophilic attractive forces can destabilize high-order collagen structures in native and *in vitro* tissues as observed microscopically[28] and ultrastructurally[68].

Measured chemical solubility predicts a chemical's ability to clear skin tissue. Our data indicate that a chemical agent's ability to suppress hydrogen-bond-mediated attractive forces within collagen directly correlates with its optical clearing potential (OCP). Traditionally, refractive index matching with collagen (n=1.45-1.55) had been used empirically to screen and select potential chemical agents for tissue optical clearing[22-24-25]. The propanediols used in our study had similar physical properties including molecular weight, index of refraction, and osmolality, but the most important predictive characteristic of their OCP was collagen solubility. Similar comparisons can be made with the sugar alcohol series; no correlation can be made between the chemical agent's index of refraction or osmolality with its OCP. For sugar alcohols, our study suggests that an even higher OCP may be realized by extending chain length.

Large chain length sugars were found to have characteristically large collagen solubilities. Dextrose and fructose had collagen solubilities similar to sorbitol whereas sucrose had the largest collagen solubility measured. Sucrose is a disaccharide composed of the two monosaccharide units dextrose and fructose bound together by a glycosidic bond. We propose that in solution, collagen molecules are free to interact with both disaccharide units of sucrose, enhancing solubility. This increase in solubility did not correlate with an increase in OCP however. We hypothesize that sterics play a role in skin clearing. In skin, interaction of sucrose with high-order collagen structures

is sterically hindered to individual monosaccharide units resulting in an OCP similar to that of dextrose and fructose.

Previous studies have reported similar relative OCP of agents to those shown herein. For example, 7 M glucose was shown to have the same optical clearing effect as 13 M glycerol as measured by fluorescence through in vitro skin[3]. This is consistent with our study in which collagen solubility predicted glucose to have twice the OCP of glycerol. In addition, it is interesting to note that in efforts to develop non-invasive, optical monitoring of blood glucose levels, a correlation has been reported between a reduction in tissue light scattering and glucose concentration[6-84-85]. The reduction in tissue scattering was hypothesized to arise from an increase in glucose concentration in local extracellular space, increasing its refractive index to better match that of tissue scatterers. The results presented here suggest that the molecular interaction of sugars as well as other chemical agents such as sugar alcohols and propanediols will lead to a reduction in tissue optical scattering.

The correlation between collagen solubility and OCP in native skin for sugars and sugar alcohols suggest that the primary characteristic of effective clearing agents is collagen affinity. High affinity allows the agents to interact efficiently with collagen and remove water. A primary physical property (collagen solubility) has been identified of effective clearing agents for tissue optical clearing. It has been shown that the ability to screen non-covalent intermolecular forces which drive collagen fibrillogenesis correlates with OCP in native skin. This property provides a criterion for selection and a basis for the rational design of optimized optical clearing agents.

CHAPTER VII

DEHYDRATION OF DERMAL COLLAGEN

7.1 Raman in Biological Applications

Raman spectroscopy has become an increasingly popular technique applied to biomedical problems. Previous studies used Raman to examine interactions of chemicals such as glycerol and water[86-88], the hydration and structure of collagen[89], and the effects of fixatives on fibrous collagen[40-43-90]. Herein the kinetics of collagen dehydration of native and fixed rodent skin was examined using Raman spectroscopy.

7.2 Raman Spectroscopy

Raman spectroscopy is fundamentally based on Raman scattering. Earlier, light scattering was described as emitted light resulting from the interaction of an incident light wave and matter. When light interacts with particles such as molecules that are smaller than its wavelength three types of scattering events result:

1. Rayleigh scattering – Elastic scattering event where emitted light is same frequency as incident light.
2. Stokes Raman Scattering – Inelastic scattering event where emitted light is of a lower frequency than the incident light.
3. Anti-Stokes Raman Scattering – Inelastic scattering event where emitted light is of a higher frequency than incident light.

Rayleigh scattering is the predominant form of scattering with the majority of scattering events being elastic. Raman scattering occurs less frequently than Rayleigh scattering but can provide molecular information of the scatterer.

The Raman scattering effect results from the interaction of incident light and electrons in the illuminated molecules. In non-resonant Raman scattering, the incident light does not have enough energy to excite the electron into a higher electronic energy level. Thus the electron is promoted to a different vibrational level within the same electronic state (Figure 27).

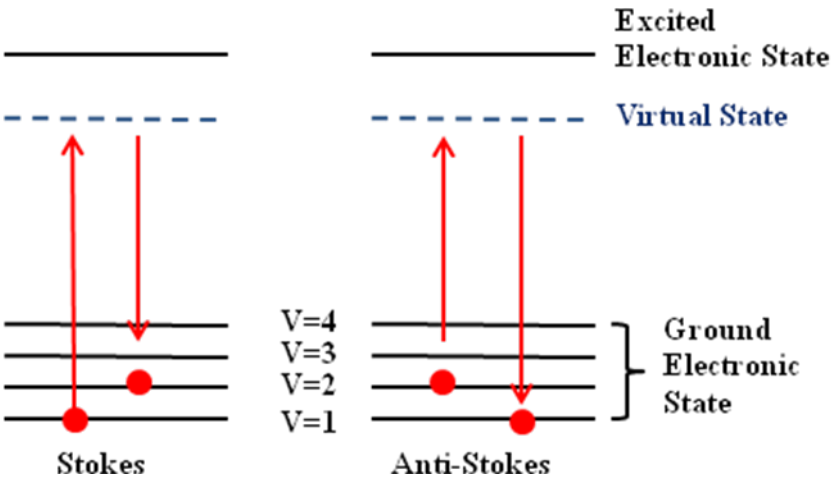

Figure 27: Energy diagram of inelastic Raman scattering. Scattered light energy is either lower (Stokes) or higher (Anti-Stokes) than incident light.

In order for a molecule to exhibit the Raman effect, incident light must induce a dipole moment in the molecule or induce a change in molecular polarizability. Light

scattered through the Raman process can be either lower or higher energy than the light incident on the molecule. When a molecule interacts with an incident photon, some of the electrons in the molecule convert the light energy into vibrational energy. The scattered light loses energy equivalent to the change in vibrational mode (Stokes Raman effect). If the electron is already in an elevated vibrational state, energy is donated, increasing the overall energy of the scattered photon (Anti-Skokes Raman effect). It is important to remember that the majority of scattered light is of the same energy as the incident photon (Rayleigh Scattering) with Raman scattering lines potentially only 10^{-6} of the intensity of the Rayleigh line.

The difference in frequency for Stokes and Anti-Stokes scattering is symmetrical. The disparity between the incident light frequency (Rayleigh scattered light) and scattered frequency in Stokes and Anti-Stokes scattering is identical (Figure 28). For a mathematical discussion of Raman scattering see the appendix. The Raman shift is independent of light source. For the sample seen in Figure 28 one would get a 600 cm^{-1} Raman shift regardless of light source wavelength. For this reason raman bands are reported as a wavenumber rather than wavelength. Modern Raman systems automatically give the wavenumber shifts which contain the biologically important information. The wavenumber is the number of waves (periods) of a given wavelength in 1 cm. The wavenumber is expressed in inverse centimeters (cm^{-1}) and has the following relationship to wavelength:

$$\nu_{WN} = \frac{1}{\lambda} = \frac{\nu}{c} \qquad 7.1$$

where ν_{WN} is the wavenumber, λ is the wavelength, and c is the speed of light.

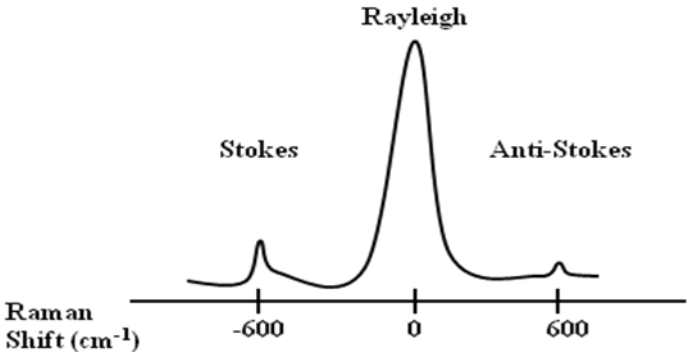

Figure 28: Raman frequency difference between Stokes and Anti-Stokes is symmetrical.

As molecular weight increases, the number of atoms present in the molecule increases as well. Increasing molecular size leads to additional vibrational modes which add to the complexity of the system. Sub-molecular groups of atoms within molecules usually appear with characteristic group frequency vibrations. For example the bond between the oxygen and hydrogen in a hydroxyl group (-OH) usually has a stretching vibration in the region of 3100-3600 cm^{-1}.

7.3 Methods of Raman Spectroscopy in Cleared Rodent Tissues

Our previous results indicate the hydration state of collagen dictates the optical properties of the tissue as a whole. Water can be divided into three categories in rodent skin: structural, bound, and free. "Structural water" is believed to stabilize collagen triple helices through interactions with its backbone. "Bound water" refers to the water between the triple helices and microfibrils. The third category of "free water" refers to the water found throughout the rest of the tissue. Clearing agents act as dehydrating agents by removing water as they infiltrate rodent skin. The exchange of water and clearing agents within collagen fibers has been implicated as the mechanism for bulk skin clearing. Raman spectroscopy was used to investigate changes in the hydration state of native and glutaraldehyde fixed, excised rodent skin dehydrated by a series of clearing agents.

Ex vivo rodent skin (3-6 wk old Sprague-Dawley) was cut into 1.0x1.0 cm^2 samples using surgical scissors. Subcutaneous fat was removed using a razorblade and rodent skin stored in 99.9 % deuterium oxide for 24 hr. Deuterium oxide (D_2O) quickly replaces water in native rodent skin and provides a unique Raman band (2250-2800 cm^{-1}) not found in native or fixed rodent skin. The unique Raman signature of D_2O allows quantitative examination of the dehydration of native and fixed rodent skin due to clearing agents. D_2O loss form clearing agent induced dehydration results in decreasing D_2O Raman band areas. Following skin immersion in D_2O, the excised skin was randomly divided into two groups: native and fixed. Fixation was carried out in 0.10,

0.25, and 0.50% vol./vol.glutaraldehyded in D_2O for 48 hrs and at a pH of 7.2 and 27 ℃. After chemical treatment, excess glutaraldehyde was rinsed off using D_2O at 27 ºC.

7.3.1 Dehydration of Fixed Rodent Skin

Raman spectra were collected for native and fixed rodent skin before and after 1 hr of immersion in 3.5 M concentrations of the clearing agents ethylene glycol, glycerol, and high fructose corn syrup (HFCS).

7.3.2 Kinetics of Dehydration

The dynamics of dehydration were examined using the clearing agents 1,3-propanediol and 1,2-propanediol (3.5 M). Native and glutaraldehyde fixed (0.10, 0.25, and 0.50 % vol/vol) rodent tissue in D_2O at a pH of 7.2 and 27 ℃ was immersed in each clearing agent with D_2O Raman band measurement at 5 min intervals for a total of 20 min for native skin and 10 min intervals for a total of 120 min for fixed skin.

7.3.3 Raman Spectra

Raman spectra was collected using a LabRam Raman spectrometer (Jobin-Yvon-Horriba) comprising an Olympus BX41 confocal microscope, 50x objective, 633 nm excitation laser, and CCD detector. Samples were placed on a glass slide and care was taken to prevent heating and dehydration of sample from the laser source or air. Keeping the laser source exiting the objective at or below 3 mW does not change the Raman spectra and prevents heating of the sample[40-43]. The spectra were recorded

using a 300 gr/mm grating, 5 scans per spectra with an integration time of 15 seconds per scan. Ten measurements were taken from the dermal side per skin sample and each spectrum averaged to accommodate the natural heterogeneity of the dermis. Baselines were adjusted using an 8^{th} order polynomial fit with native and fixed skin Raman bands normalized.

7.4 Raman Spectra Controls

Several controls were implemented to get an accurate measurement of water loss in native and fixed rodent dermis. D_2O was selected to track water loss in tissue due to its unique properties. First, D_2O is similar to water and quickly exchanges with free and bound water in collagen[40-43]. D_2O also exhibits a unique Raman band in from 2200 cm^{-1} to 2800 cm^{-1} not found in either native tissue, fixed tissue, or the clearing agents examined in this study (Figure 29).

Figure 29 shows the Raman spectra for native rodent skin immersed in H_2O, PBS, and 3.5 M glycerol for 24 hrs. No band is seen in the reported wavenumber range for D_2O (2200-2800 cm^{-1}) in any skin sample. Introduction of the clearing agent increased the (CH) band characteristic of the addition of sugar alcohol.

Figure 30 shows the Raman intensity spectra for native skin immersed in D_2O for 24 hr prior to fixation with increasing concentrations of glutaraldehyde. The Raman band characteristic of D_2O is present. The marked increase of D_2O band area with increasing amounts of glutaraldehyde is expected and agrees with previous studies that found GA increases the amount of bound water within collagen fibers.

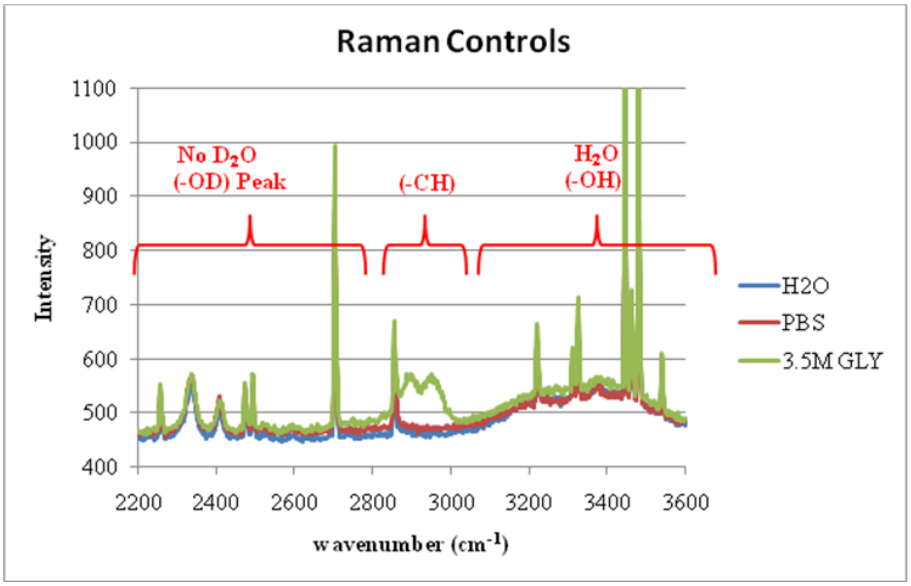

Figure 29: Raman spectra of native skin previously immersed in water, PBS, and 3.5 M glycerol for 1 hr. No Raman bands are seen in the 2200-2800 cm^{-1} range.

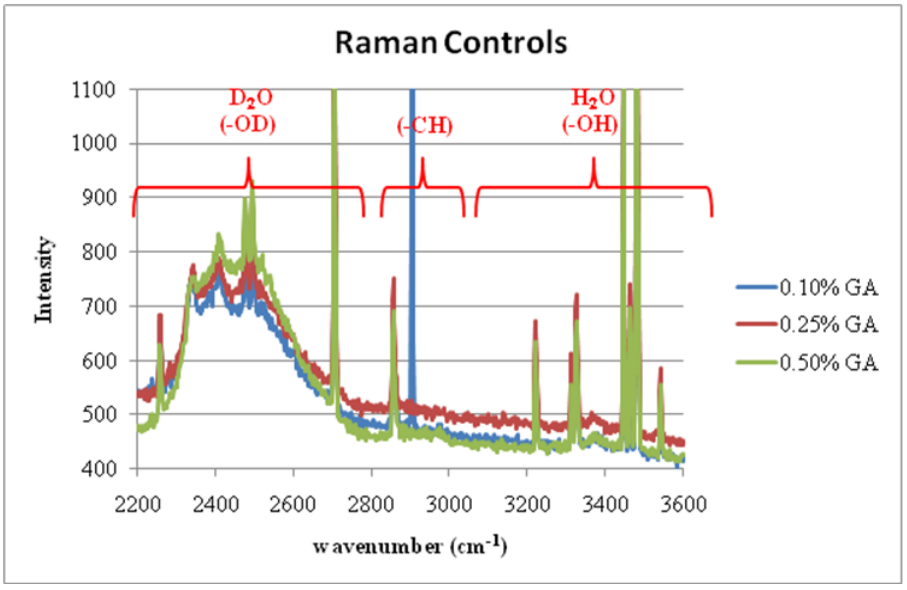

Figure 30: Raman spectra of rodent skin immersed in D_2O for 24 hr followed by fixation with 0.10%, 0.25%, and 0.50% solutions of glutaraldehyde and D_2O. Notice the Raman band characteristic of D_2O in the 2200-2800 cm^{-1} region.

7.5 Raman Spectroscopy in Cleared Rodent Tissues

Deuterium oxide (D_2O) is freely interchangeable with water in skin and exhibits an OD Raman band from 2200 cm^{-1} to 2800 cm^{-1}. Skin fixed in 0.10%, 0.25%, and 0.50% gluaraldehyde with D_2O was immersed in 3.5M ethylene glycol, glycerol, and high fructose corn syrup (HFCS) for 1 hr and is shown in Figure 31. Each clearing agent fully removed all measurable D_2O from native skin after 1 hr (data not shown). Raman OD band areas were normalized and presented as a percentage of the initial, fully hydrated skin D_2O peak area. OD band area fell in response to dehydration. D_2O was progressively retained upon dehydration with increasing glutaraldehyde concentration. High fructose corn syrup was the most effective dehydrating agent followed by glycerol and ethylene glycol. Glutaraldehyde crosslinks hinder the clearing agents' ability to remove water as seen for 0.25% and 0.50% GA fixed tissues. This finding is consistent with previously reported studies which found reduced water exchange in GA fixed tissues[91-92].

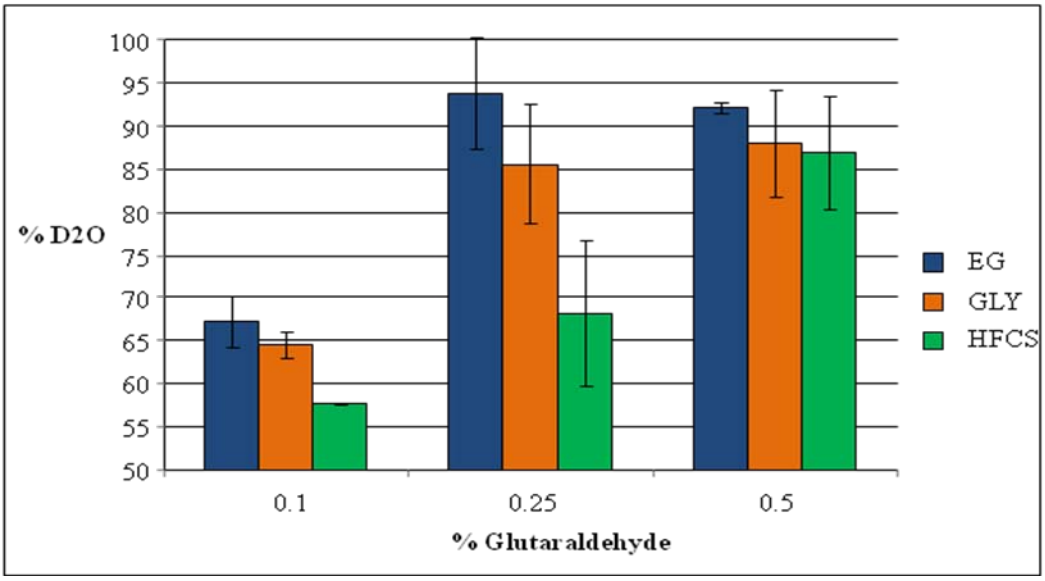

Figure 31: Percent D_2O remaining in fixed skin after immersion in ethylene glycol, glycerol, and high fructose corn syrup (HFCS). Increases in glutaraldehyde concentration leads to greater water retension.

Raman spectroscopy was used to assess the degree of water loss due to clearing agent infiltration in fixed skin tissue. Increasing concentrations of the fixative glutaraldehyde (GA) slowed water removal when dehydrated with hyper-osmotic agents. Just over half of the D_2O remained in the tissue after 1 hr of dehydration in 0.10% GA fixed skin. Increasing the concentration of GA lead to greater D_2O retention with very little D_2O loss in 0.50% GA fixed skin. Interactions between glutaraldehyde and collagen explain slow water loss. Cheung et al. suggested that glutaraldehyde forms a barrier around the outermost layer of collagen that could slow diffusion in and out of the protein[93]. Jastrzebska et al, found that the GA cross linking process lead to increased water molecules in the hydration shell around collagen triple helices that were not freely

exchanged[91]. This barrier effect could explain the increasing inability of hyper-osmotic chemical agents to remove water from fixed tissue.

Interestingly, the ability to dehydrate fixed skin correlates with collagen solubility and clearing potential. High fructose corn syrup (HFCS) was the most effective dehydrating agent followed by glycerol and ethylene glycol. Our previous studies indicated that fructose was an efficient clearing agent with high collagen solubility when compared to glycerol and ethylene glycol[36-38]. The high collagen affinity of HFCS potentially leads to more efficient dehydration in fixed skin.

The kinetics of skin dehydration due to clearing agents were examined. Figure 32-35 are bar graphs depicting the decrease in D_2O band area for native and 0.10, 0.25, and 0.50 % GA fixed skin immersed in 1,2-propanediol and 1,3-propanediol over time. Native rodent skin and 0.10%, 0.25%, and 0.50% glutaraldehyde with D_2O fixed skin were dehydrated for 120 min by 1,2-propanediol and 1,3-propanediol. After 10 min of immersion in 3.5M 1,3-propanediol, native rodent skin had a significantly reduced D_2O concentration compared to that immersed in 1,2-propanediol (Figure 32). 0.10% glutaraldehyde fixed skin showed a similar, but delayed trend with 1,3-propanediol exhibiting greater dehydration effects 20 min after application (Figure 33). Higher concentrations of glutaraldehyde (0.25% and 0.50%) fixed rodent skin showed larger D_2O retention with little difference between the propanediols to remove water (Figures 34 & 35).

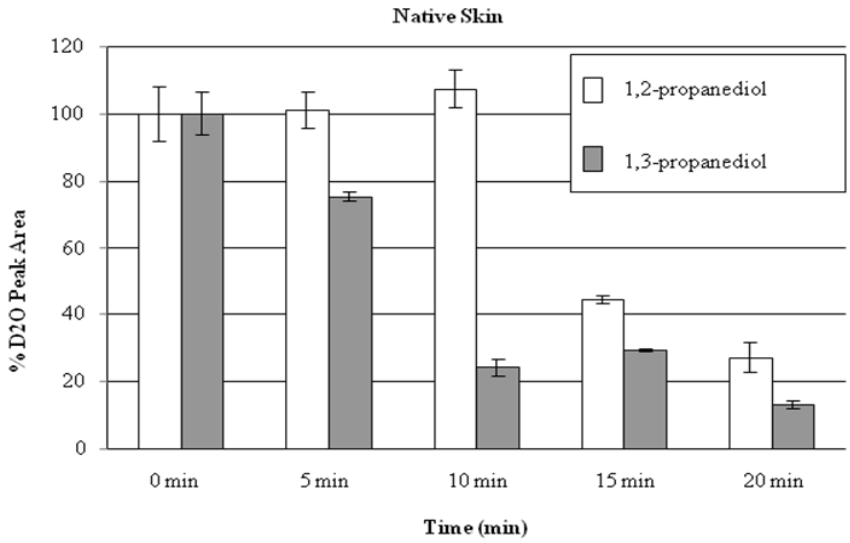

Figure 32: Percent D_2O remaining in native skin after immersion in 1,2-propanediol and 1,3-propanediol. 1,3-propanediol was found to be a more effective dehydrating agent.

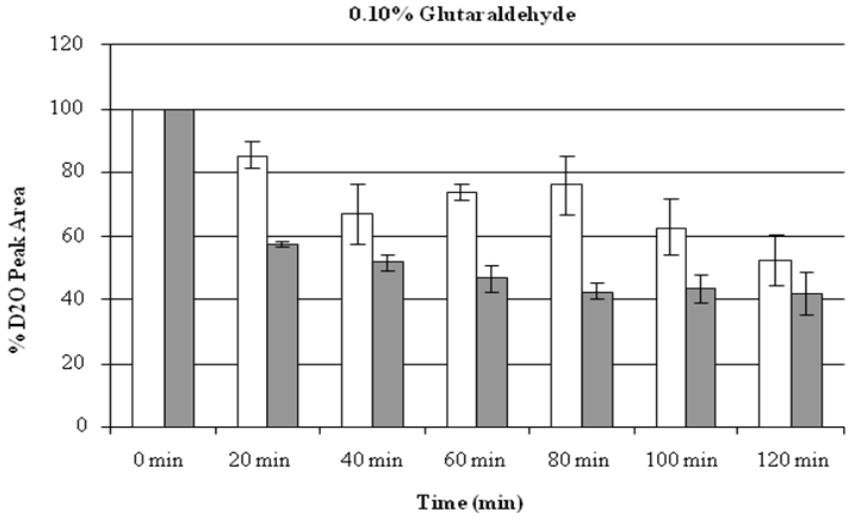

Figure 33: Percent D_2O remaining in 0.10% fixed skin after immersion in 1,2-propanediol and 1,3-propanediol. 1,3-propanediol was found to be a more effective dehydrating agent.

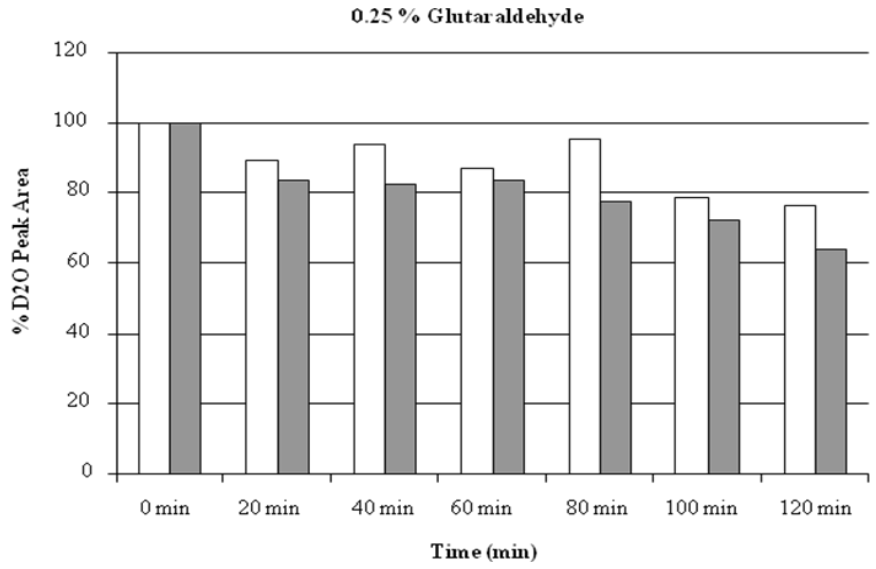

Figure 34: Percent D_2O remaining in 0.25% fixed skin after immersion in 1,2-propanediol and 1,3-propanediol.

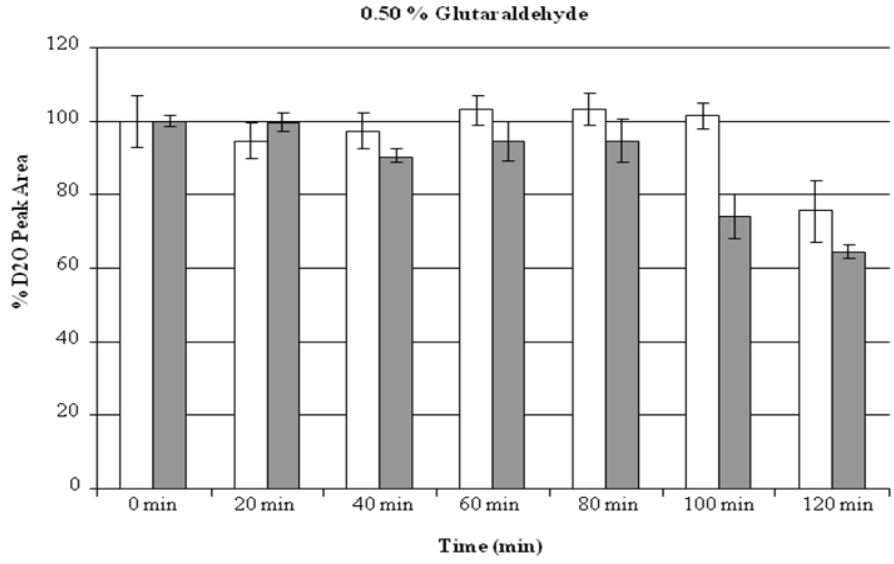

Figure 35: Percent D_2O remaining in 0.50% fixed skin after immersion in 1,2-propanediol and 1,3-propanediol.

Collagen affinity plays an important role in chemical agent dehydration of tissue. The kinetics of dehydration were examined using a pair of propanediols. Native and fixed rodent skin was dehydrated for 120 min by 1,3-propanediol and 1,2-propanediol. Comparable osmolality of each agent would suggest an equivalent ability to dehydrate fixed tissue. 1,3-propanediol was found to dehydrate native and 0.10% fixed skin more effectively than 1,2-propanediol. As illustrated in chapter IV, hydroxyl group placement plays a critical role in interactions between clearing agents and collagen triple helices[38]. The larger spacing between hydroxyl groups in 1,3-propanediol allows it to form additional hydrogen bonds with collagen. The greater collagen affinity of 1,3-propanediol led to more efficient dehydration of skin.

CHAPTER VIII

CONCLUSION

8.1 The Clearing Mechanism

The findings presented in this work suggest that the mechanism of skin optical clearing incorporates aspects of all three previously proposed mechanisms: dehydration, refractive index matching, and collagen dissociation. Tuchin first proposed dehydration and refractive index matching as the primary cause of tissue clearing by suggesting that clearing agent removal of bulk water reduces the refractive index mismatch between collagen fibers and the surrounding media[1]. Since Tuchin's initial clearing proposal, several studies have examined clearing in tissue in an effort to further define the clearing mechanism. Vargas suggested that index matching in concert with dehydration cleared tissue allowing a greater amount of florescent signal to be recovered from beneath skin.[3] Other studies by Rylander[23], Xu[10-12], and Wang[9], implicated dehydration alone as the sole cause of tissue transparency.

Refractive index matching and dehydration was found lacking as the primary cause of tissue clearing when Choi et al illustrated that clearing agent physical properties such as refractive index and osmolality do not correlate with an agent's ability to clear skin.[27] Additionally, Yeh et al. discovered that molecular interactions between clearing agents and collagen perturb the native collagen structure during the clearing process suggesting a molecular mechanism for clearing[28]. In totality, these results

illustrate that clearing is a dynamic process with each study described above shedding light on a single aspect of the clearing process.

The work presented in this dissertation suggests a unified clearing mechanism containing aspects of all three previous hypotheses of tissue clearing. Clearing was found to be a complex process with thermodynamic and kinetic components. First, there is a thermodynamic equilibrium that is reached between clearing agents and skin. Concentration gradients drive clearing agents to diffuse into skin and remove water. The introduction of clearing agents into the tissue begins to optically homogenize skin and reduce light scatter. Interestingly, this process does not seem sensitive to small variations in clearing agent refractive index. No differences in clearing ability of the agents examined herein were found yet their refractive indices ranged from 1.42 to 1.47. Secondly, there is kinetic component to clearing. Chemical agents clear skin with differing rates. The speed of clearing was found to increase with molecular size and number of hydroxyl groups. This finding points to molecular interactions between clearing agents and collagen as a major component of clearing.

The molecular modeling program CHARMM suggests collagen affinity plays a major role in clearing agents ability to interact with collagen and remove bound water. Clearing agents interact with collagen triple helices through hydrogen bonding and bridging thereby disrupting the water hydration shell surrounding collagen molecules. A correlation was found between clearing efficacy and the ability of clearing agents to hydrogen bond with collagen (collagen affinity). Increases in clearing agent molecular

size and hydroxyl groups led to a higher affinity for collagen and more effective tissue optical clearing.

Collagen solubility is a measure of clearing agent affinity for collagen and was found as a predictor of measured OCP. Computational molecular modeling predictions were confirmed experimentally using collagen fibrillogenesis inhibition and solubility measurements. Clearing agents have an affinity for collagen molecules and shield the attractive forces between collagen triple helices reducing fibrillogenesis. Increasing clearing agent molecular size led to a greater reduction of fibrillogenesis with corresponding high collagen solubility. High collagen solubility was a physical characteristic of the most effective clearing agents that was found to predict optical clearing efficacy.

Clearing was hypothesized as optically homogenizing skin by clearing agent removal of bound water between collagen triple helices. Raman spectroscopy is capable of investigating the hydration state of dermal collagen fibers. Deuterium oxide (D_2O) in concert with Raman spectroscopy quantified clearing agent induced dehydration of dermal collagen. Clearing agent ability to dehydrate dermal collagen corresponded with collagen affinity and the ability to optically clear tissues. The most effective clearing agents were found to remove bound water with the greatest efficacy.

The replacement of bound water by clearing agents with an index of refraction similar to collagen optically homogenizes skin tissue leading to a reduction in light scattering. Previous suggestions of index matching and dehydration of collagen were incomplete. Replacement of collagen fiber's surrounding medium with a high index

material is not sufficient to induce a large amount of optical clearing in skin. Our results suggest a molecular mechanism for clearing. Collagen fibers must be homogenized by clearing agent removal of bound water between triple helices and fibrils. Through dehydration of collagen with concomitant diffusion of clearing agent into collagen, the skin is homogenized leading to a large reduction in tissue light scattering.

REFERENCES

1. Tuchin V. V., Maksimova I. L., Zimnyakov D. A., Kon I. L., Mavlutov A. H. and Mishin A. A. Light propagation in tissues with controlled optical properties. Journal of Biomedical Optics 1997;2:401-417.

2. Vargas G., Chan E. K., Barton J. K., Rylander H. G., III and Welch A. J. Use of an agent to reduce scattering in skin. Lasers in Surgery and Medicine 1999;24:133-141.

3. Vargas G., Chan K. F., Thomsen S. L. and Welch A. J. Use of osmotically active agents to alter optical properties of tissue: Effects on the detected fluorescence signal measured through skin. Lasers in Surgery and Medicine 2001;29:213-220.

4. Khan M. H., Chess S., Choi B., Kelly K. M. and Nelson J. S. Can topically applied optical clearing agents increase the epidermal damage threshold and enhance therapeutic efficacy? Lasers in Surgery and Medicine 2004;35:93-95.

5. Khan M. H., Choi B., Chess S., Kelly K. M., McCullough J. and Nelson J. S. Optical clearing of *in vivo* human skin: Implications for light-based diagnostic imaging and therapeutics. Lasers in Surgery and Medicine 2004;34:83-85.

6. Maier J. S., Walker S. A., Fantini S., Franceschi M. A. and Gratton E. Possible correlation between blood glucose concentration and the reduced scattering coefficient of tissues in the near infrared. Optics Letters 1994;19:2062-2064.

7. Wang R. K. Signal degradation by multiple scattering in optical coherence tomography of dense tissue: A Monte Carlo study towards optical clearing of biotissues. Physics in Medicine and Biology 2002;47:2281-2299.

8. Wang R. K., Xu X., He Y. and Elder J. B. Investigation of optical clearing of gastric tissue immersed with hyperosmotic agents. IEEE Journal of Selected Topics in Quantum Electronics 2003;9:234-242.

9. Wang R. K., Xu X., Tuchin V. V. and Elder J. B. Concurrent enhancement of imaging depth and contrast for optical coherence tomography by hyperosmotic agents. Journal of Optical Society of America B 2001;18:948-953.

10. Xu X. and Wang R. K. The role of water desorption on optical clearing of biotissue: Studied with near infrared reflectance spectroscopy. Medical Physics 2003;30:1246-1253.

11. He Y. and Wang R. K. Dynamic optical clearing effect of tissue impregnated with hyperosmotic agents and studied with optical coherence tomography. Journal of Biomedical Optics 2004;9:200-206.

12. Xu X. and Wang R. K. Synergistic effect of hyperosmotic agents of dimethyl sulfoxide and glycerol on optical clearing of gastric tissue studied with near infrared spectroscopy. Physics in Medicine and Biology 2004;49:457-468.

13. Lanigan S. W., J.A. Cotterill. Psycological disabilities amongst patients with port wine stains. British Journal of Dermatology 1989;121:209-215.

14. Pratt A. G. Birthmarks in infants. Archives of Dermatology Syphilol. 1953;67:302-305.

15. Milliken J. B. and Young A. R. Vascular birthmarks - hemangiomas and malformations: New York: Oxford University Press. 1988

16. Jacobs A. H. and Walton R. G. The incidence of birthmarks in the neonate. Pediatrics 1976;58:218-222.

17. Malm M. and Calber M. N. Port-wine stain - a surgical and psychological problem. Ann. Plast. Surg. 1988;20:512-516.

18. Kalick S. M. Toward an interdisciplinary psychology of appearances. Psychiatry 1978;41: 243-253.

19. Heller M., Rafman S., Svagulis I. and Pless I. B. Birth defects and psychosocial adjustment. Am. J. Dis. Child 1985;139:257-263.

20. Geronemus R. G. and Ashinoff R. The medical necessity of evaluation and treatment of port-wine stains. J. Dermatol. Surg. Oncol. 1991;17:76-79.

21. Lever W. F. and Schaumburg-Lever G. Histopathology of the skin (7th ed.): Philadelphia, PA: J.B. Lippincott Company. 1990

22. Saidi I. S., Jacques S. L. and Tittel F. K. Mie and Rayleigh modeling of visible-light scattering in neonatal skin. Applied Optics 1995;34:7410-7418.

23. Rylander C. G., Stumpp O., Milner T., Kemp N. J. and Mendenhall J. M. Dehydration mechanism of optical clearing in tissues. Journal of Biomedical Optics 2006;11:041117.

24. Tuchin V. V. Optical clearing of tissues and blood: Belhaven, WA: SPIE - The International Society for Optical Engineering. 2005

25. Gisselberg M., Clark J. I., Vaezy S. and Osgood T. B. A quantitative evaluation of fourier components in transparent and opaque calf cornea. American Journal of Anatomy 1991;191:408-418.

26. Vargas G., Readinger A., Dozier S. S. and Welch A. J. Morphological changes in blood vessels produced by hyperosmotic agents and measured by optical coherence tomography. Photochemistry and Photobiology 2003;77:541-549.

27. Choi B., Tsu L., Chen E., Ishak T. S., Iskandar S. M., Chess S. and Nelson J. S. Determination of chemical agent optical clearing potential using *in vitro* human skin. Lasers in Surgery and Medicine 2005;36:72-75.

28. Yeh A. T., Choi B., Nelson J. S. and Tromberg B. J. Reversible dissociation of collagen in tissues. Journal of Investigative Dermatology 2003;121:1332-1335.

29. Hayashi T. and Nagai Y. Factors affecting the interactions of collagen molecules as observed by *in vitro* fibril formation. Journal of Biochemistry 1972;72:749-758.

30. Yannas I. V. Collagen and gelatin in the solid state. Journal of Macromolecular Science - Reviews in Macromolecular Chemistry 1972;C7:49-104.

31. Prahl S., van Gemert M. and Welch A. Determining the optical properties of turbid media by using the adding-doubling method. Applied Optics 1993;32:559-568.

32. Prahl S. Ch. 5: The adding-doubling method: Portland, OR: Plenum Press. 1995

33. Pickering J. W., Prahl S., van Wieringen N., Beek J. B., Sterenborg H. J. C. M. and van Gemert M. Double integrating sphere system for measuring optical properties of tissue. Applied Optics 1993;32:399-410.

34. McNichols R. J., Fox M. A., Gowda A., Tuya S., Bell B. and Motamedi M. Temporary dermal scatter reduction: Quantitative assessment and implications for improved laser tattoo removal. Lasers in Medical Science 2005;36:289-296.

35. Wells P. B., Yeh A. T. and Humphrey J. D. Influence of glycerol on the mechanical behavior and thermal damage susceptibility of collagenous tissues. IEEE Transactions on Biomedical Engineering 2006;53:747-753.

36. Hirshburg J., Choi B., Nelson J. S. and Yeh A. T. Correlation between collagen solubility and skin optical clearing using sugars. Lasers in Surgery and Medicine 2007;39:140-144.

37. Tuchin V. V., Altshuler G., Gavrilova A., Pravdin A., Tabatadze D., Childs J. and Yaroslavsky I. Optical clearing of skin using flashlamp-induced enhancement of epidermal permeability. Lasers in Surgery and Medicine 2006;38:824-836.

38. Hirshburg J., Choi B., Nelson J. S. and Yeh A. T. Collagen solubility correlates with skin optical clearing. Journal of Biomedical Optics 2006;11:040501.

39. Rosner B. Fundamentals of biostatistics: Pacific Grove, CA: Duxbury Thomas Learning. 2000

40. Jastrzebska M., Wrzalik R., Kocot A., Zalewska-Rejdak J. and Cwalina B. Hydration of glutaraldehyde-fixed pericardium tissue: Raman spectroscopic study. J. Raman Spectroscopy 2003;34:424-431.

41. Fathima N., Madhan B., Rao J., Nair B. and Ramasami T. Interaction of aldehydes with collagen: Effect on thermal, enzymatic and conformational stability. Biological Macromolecules 2004;34:241-247.

42. Cheung D., Perelman N., Ko E. and Nimni M. Mechanism of crosslinking of proteins by glutaraldehyde iii. Connective Tissue Research 1985;13:109-115.

43. Jastrzebska M., Wrzalik R., Kocot A., Zalewska-Rejdak J. and Cwalina B. Raman spectroscopic study of glutaraldehyde-stabilized collagen and pericardium tissue. J. Biomaterials Science 2003;14:185-197.

44. Olde Damink L., Dikstra P., Van Luyn M., Van Wachem P., Nieuwenhuis P. and Feijen J. Glutaraldehyde as a crosslinking agent for collagen-based biomaterials. J. Material Science: Materials in Medicine 1995;6:424-431.

45. Allen M. and Tildesley D. Computer simulation of liquids: New York: Oxford University Press. 1989

46. Brooks B., Bruccoleri R., Olafson B., States D., Swaminathan S. and Karplus M. A program for macromolecular energy, minimization, and dynamics calculations. Journal of Computational Chemistry B 1983;4:187-217.

47. MacKerell A., Bashford D., Bellott M., Dunbrack R., Evanseck J., Field M., Fischer S., Gao J., Guo H., Ha S., Joseph-McCarthy D., Kuchnir L., Kuczera K., Lau F., Mattos C., Michnick S., Ngo T., Nguyen D., Prodhom B., Reiher III W., Roux B., Schlenkrich M., Smith J., Stote R., Straub J., Watanabe M., Wiorkiewicz-Kuczera J., Yin D. and Karplus M. All-atom empirical potential for molecular modeling and dynamics studies of proteins. Journal of Physical Chemistry 1998;102:3586-3616.

48. Kramer R., Bella J., Mayville P., Brodsky B. and Berman H. Sequence dependant conformational variations of collagen triple-helical structure. Nature Structural Biology 1999;6:454-457.

49. Ravikumar K. and Hwang W. Region-specific role of water in collagen unwinding and assembly. Proteins 2008;72:1320-1332.

50. Rainey J. and Goh M. An interactive triple-helical collagen builder. Bioinformatics 2004;20:2458-2459.

51. Brunger A. and Karplus M. Polar hydrogen positions in proteins: Empirical energy placement and neutron diffraction comparison. Proteins 1988;4:148-156.

52. Anderson D. Collagen self-assembly: A complementary experimental and theoretical perspective. PhD Thesis. Univ. Toronto, Toronto, Canada. 2005

53. Im W., Lee M. and Brooks C. Generalized born model with a simple smoothing function. Journal of Computational Chemistry 2003;24:1691-1702.

54. De Loof H., Nilsson L. and Rigler R. Molecular dynamics simulation of galanin in aqueous and nonaqueous solution. Journal of the American Chemical Society 1992;114:4028-4035.

55. Hirshburg J., Choi B., Nelson J. and Yeh A. Collagen solubility correlates with skin optical clearing. Journal of Biomedical Optics 2006;11:040501.

56. Campagnola P. J. and Loew L. M. Second-harmonic imaging microscopy for visualizing biomolecular arrays in cells, tissues and organisms. Nature Biotechnology 2003;21:1356-1360.

57. Zipfel W. R., Williams R. M. and Webb W. W. Nonlinear magic: Multiphoton microscopy in the biosciences. Nature Biotechnology 2003;21:1369-1377.

58. Boyd R. W. Nonlinear optics: San Diego, CA: Elsevier Science (USA). 2003

59. Zoumi A., Yeh A. T. and Tromberg B. J. Imaging cells and extracellular matrix *in vivo* by using second-harmonic generation and two-photon excited fluorescence. Proceedings of the National Academy of Sciences 2002;99:11014-11019.

60. Yeh A. T., Nassif N., Zoumi A. and Tromberg B. J. Selective corneal imaging using combined second harmonic generation and two-photon excited fluorescence. Optics Letters 2002;27:2082-2084.

61. Yeh A. T., Hammer-Wilson M. J., Van Sickle D. C., Benton H. P., Zoumi A., Tromberg B. J. and Peavy G. M. Nonlinear optical microscopy of articular cartilage. Osteoarthritis and Cartilage 2005;13:345-352.

62. Hulmes D. J. S. Building collagen molecules, fibrils, and suprafibrillar structures. Journal of Structural Biology 2002;137:2-10.

63. Engel J. and Prockop D. J. The zipper-like folding of collagen triple helices and the effects of mutations that disrupt the zipper. Annual Review of Biophysics and Biophysical Chemistry 1991;20:137-152.

64. Nimni M. E. Collagen: Structure, function, and metabolism in normal and fibrotic tissues. Seminars in Arthritis and Rheumatism 1983;13:1-85.

65. Theodossiou T., Rapti G. S., Hovhannisyan V., Georgiou E., Politopoulos K. and Yova D. Thermally induced irreversible conformational changes in collagen probed by optical second harmonic generation and laser-induced fluorescence. Lasers in Medical Science 2002;17:34-41.

66. Yeh A. T., Kao B., Jung W. G., Chen Z., Nelson J. S. and Tromberg B. J. Imaging wound healing using optical coherence tomography and multiphoton microscopy in an *in vitro* skin-equivalent tissue model. Journal of Biomedical Optics 2004;9:248-253.

67. Lin S.-J., Hsiao C.-Y., Sun Y., Wen L., Lin W.-C., Jan G.-J., Jee S.-H. and Dong C.-Y. Monitoring the thermally induced structural transitions of collagen by use of second-harmonic generation microscopy. Optics Letters 2005;30:622-624.

68. Leonardi L., Ruggeri A., Roveri N., Bigi A. and Reale E. Light microscopy, electron microscopy, and x-ray diffraction analysis of glycerinated collagen fibers. Journal of Ultrastructure Research 1983;85:228-237.

69. Russell A. E. Effect of alcohols and neutral salt on the thermal stability of soluble and precipitated acid-soluble collagen. Biochemistry Journal 1973;131:335-342.

70. Miles C. A. and Burjanadze T. V. Thermal stability of collagen fibers in ethylene glycol. Biophysical Journal 2001;80:1480-1486.

71. Na G. C. Interaction of calf skin collagen with glycerol: Linked function analysis. Biochemistry 1986;25:967-973.

72. Prockop D. J. and Fertala A. Inhibition of the self-assembly of collagen I into fibrils with synthetic peptides. Journal of Biological Chemistry 1998;273:15598-15604.

73. Holmgren S. K., Taylor K. M., Bretscher L. E. and Raines R. T. Code for collagen's stability deciphered. Nature 1998;392:666-667.

74. Israelachvili J. and Wennerstrom H. Role of hydration and water structure in biological and colloidal interactions. Nature 1996;379:219-225.

75. Kuznetsova N., Chi S. L. and Leikin S. Sugars and polyols inhibit fibrillogenesis of type I collagen by disrupting hydrogen-bonded water bridges between the helices. Biochemistry 1998;37:11888-11895.

76. Kuznetsova N., Rau D. C., Parsegian V. A. and Leikin S. Solvent hydrogen-bond network in protein self-assembly: Solvation of collagen triple helices in nonaqueous solvents. Biophysical Journal 1997;72:353-362.

77. Leikin S., Rau D. C. and Parsegian V. A. Direct measurement of forces between self-assembled proteins: Temperature-dependent exponential forces between collagen triple helices. Proceedings of the National Academy of Sciences 1994;91:276-280.

78. Leikin S., Rau D. C. and Parsegian V. A. Temperature-favoured assembly of collagen is driven by hydrophilic not hydrophobic interactions. Nature Structural & Molecular Biology 1995;2:205-210.

79. Na G. C., Butz L. J., Bailey D. G. and Carroll R. J. *In vitro* collagen fibril assembly in glycerol solution: Evidence for a helical cooperative mechanism involving microfibrils. Biochemistry 1986;25:958-966.

80. Parsegian V. A., Rand R. P., Fuller N. L. and Rau D. C. Osmotic stress for the direct measurement of intermolecular forces. Methods in Enzymology 1986;127:400-416.

81. Hirshburg J., Choi B., Nelson J. S. and Yeh A. T. Collagen solubility correlates with skin optical clearing. Journal of Biomedical Optics 2006; 11: 040501.

82. Yeh A. T. and Hirshburg J. Molecular interactions of exogenous chemical agents with collagen--implications for tissue optical clearing. Journal of Biomedical Optics 2006;11:014003.

83. Na G. C. Uv spectroscopic characterization of type I collagen. Collagen Related Research 1988;8:315-330.

84. Esenaliev R., Larin K., Larina I. and Motamedi M. Noninvasive monitoring of glucose concentration with optical coherence tomography. Optics Letters 2001;19:992-994.

85. Bruulsema J., Hayward J., Farrell T., Patterson M., Heinemann L., Berger M., Koschinsky T., Sandahl-Christiansen J., Orskov H., Essenpreis M., Schmelzeisne-Redeker G. and Bocker D. Correlation between blood glucose concentration in diabetics and noninvasively measured tissue optical scattering coefficient. Optics Letters 1997;22:190-192.

86. Kojima S. Anomalous behavior of the o-h stretching vibrational mode in the liquid-glass transition of glycerol. J. Molecular Structure 1993;294:193-196.

87. Mudalige A. and Pemberton J. Raman spectroscopy of glycerol/d2o solutions. Vibrational Spectroscopy 2007;45:27-35.

88. Mendelovici E., Frost R. and Klooprogge T. Cryogenic raman spectroscopy of glycerol. J. Raman Spectroscopy 2000;31:1121-1126.

89. Leikin S., Parsegian V., Yang W. and Walrafen G. Raman spectral evidence for hydration forces between collagen triple helices. Proc. Natl. Acad. Sci. 1997;94:11312-11317.

90. Tarnowski C., Stewart S., Holder K., Campbell-Clark L., Thoma R., Adams A., Moore M. and Morris M. Effects of treatment protocols and subcutaneous implantation on bovine pericardium: A Raman spectroscopy study. Journal of Biomedical Optics 2003;8:179-184.

91. Jastrzebska M., Wrzalik R., Kocot A., Zalewska-Rejdak J. and Cwalina B. Hydration of glutaraldehyde-fixed pericardium tissue: Raman spectroscopic study. J. Raman Spectroscopy 2003;34:424-431.

92. Jastrzebska M., Wrzalik R., Kocot A., Zalewska-Rejdak J. and Cwalina B. Raman spectroscopic study of glutaraldehyde-stabilized collagen and pericardium tissue. J. Biomaterials Science: Polymer Edn. 2003;14:185-197.

93. Cheung D. T., Perelman N., Ko E. C. and Nimni M. E. Mechanism of crosslinking of proteins by glutaraldehyde iii. Reactions with collagen in tissues. Connective Tissue Research 1985;13:109-115.

94. Durian D. The diffusion coefficient depends on absorption. Optics Letters 1998;23:1502-1504.

95. Ishimaru A. Diffusion of light in turbid material. Applied Optics 1989;28:2210-2215.

96. Farrell I., Patterson M. and Wilson B. A diffusion theory model of spatially resolved, steady state diffuse reflectance for the noninvasive determination of tissue optical properties *in vivo*. Medical Physics 1992;19:881-888.

97. Keijzer M., Star W. and Storchi P. Optical diffusion in layered media. Applied Optics 1988;27:1820-1824.

98. Yoon G., Prahl S. and Welch A. Accuracies of the diffusion approximation and its similarity relations for laser irradiated biological media. Applied Optics 1989;28:2250-2255.

99. Yoo K., Liu F. and Alfano R. When does the diffusion approximation fail to describe photon transport in random media? Physical Review Letters 1990;64:2647-2650.

100. Dayan I., Halvin S. and Weiss G. Photon migration in a 2-layered turbid medium- a diffusion analysis. Journal of Modern Optics 1992;39:1567-1582.

101. Erikson A., Ortegren J., Hompland T., de Lange Davies C. and Lindgren M. Quantification of the second-order nonlinear susceptibility of collagen I using a laser scanning microscope. Journal of Biomedical Optics 2007;12:044002.

102. Perkampus H. Uv-vis spectroscopy and its applications: New York: Springer. 1992

103. Smith E. and Dent G. Modern Raman spectroscopy: A practical approach: Chichester, England: John Wiley & Sons. 2005

104. Long D. The Raman effect: A unified treatment of the theory of Raman scattering by molecules: Chichester, England: John Wiley & Sons. 1977

105. Ferraro J. and Nakamoto K. Introductory Raman spectroscopy: San Diego, CA: Academic Press. 1994

APPENDIX A

INVERSE ADDING DOUBLING

Before discussing the inverse adding doubling method (IAD) we must first step back and briefly review general tissue optics. Tissue is not transparent and attenuates light. The attenuation of a collimated laser beam in a homogenous layer of tissue can be described by the exponential Beer-Lambert law:

$$I(d) = (1 - R_F) I_0 \exp(-\mu_t d) \qquad \text{A1.1}$$

where I(d) is the intensity of collimated transmitted light, R_F is the coefficient of Fresnel reflection $[(n-1)/(n+1)]^2$, n is the relative mean refractive index, I_0 is the incident light intensity, μ_t is the extinction coefficient, and d is the length of the tissue. The above equation is useful if the optical properties (μ_a, μ_s) are known but in many circumstances they are unknown and need to be calculated. The Beer-Lambert law does not allow for accurate calculations of μ_a and μ_s in tissue since multiple combinations of each coefficient would lead to similar intensity extinctions.

The inverse adding doubling method (IAD) is an effective and commonly used method to calculate each coefficient.[22-24-31] IAD uses total reflectance and total transmission to calculate the optical properties of bulk tissue. "Inverse" describes the reverse of the usual process of calculating reflection and transmission from optical properties. "Adding-doubling" indicates the way the radiative transport equation is

solved within a specified error range. The radiative transport equation (RTE) describes light propagation within tissue. The overall equation is an energy balance in the form[24]:

$$\frac{\partial I(\boldsymbol{r},\boldsymbol{s})}{\partial \boldsymbol{s}} = -\mu_t I(\boldsymbol{r},\boldsymbol{s}) + \frac{\mu_s}{4\pi}\int_{4\pi} I(\boldsymbol{r},\boldsymbol{s}')p(\boldsymbol{s},\boldsymbol{s}')d\Omega' \qquad \text{A1.2}$$

[Change of energy of area element = Energy out + Energy in]

where I(**r**,**s**) is the radiance or the amount of energy that flows across an area at point **r** in the direction of **s.** μ_t is the total attenuation ($\mu_a + \mu_s$) and p(**s**,**s'**) is a probability density function or "phase function" describing scattering in direction **s'** for a photon traveling in **s**. In practice the phase function has been found to be accurately approximated in tissue using the Henyey-Greenstein function:

$$p(\theta) = \frac{1}{4\pi}\left(\frac{1-g^2}{(1+g^2-2g\cos\theta)^{\frac{3}{2}}}\right) \qquad \text{A1.3}$$

Where g is the scattering anisotropy factor (<cosθ>) which describes the direction of scattering (-1: totally backscattered, 0: isotropic, 1: totally forward). IAD approximates the RTE to find the optical properties of the tissue.

Inverse Adding Doubling (IAD) Method of Optical Property Measurement.[32]

Assumptions:

- Continuous incident light

- Samples have homogenous optical properties
- Sample geometry is infinite plane-parallel slab with finite thickness
- Uniform index of refraction
- Light is unpolarized

IAD is an iterative method developed to approximate the solution to the radiative transport equation. The following discussion/calculations will be for the geometry:

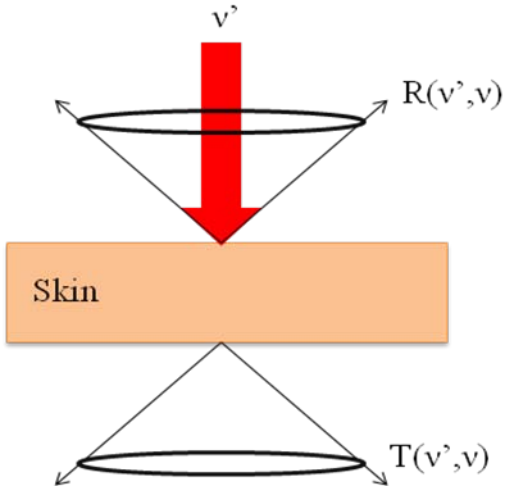

Turbid slabs transmit and reflect light at different angles. R(ν',ν) and T(ν',ν) denote total reflected and transmitted light from the slab. Total reflectance is defined by van de Hulst and Prahl [32] as:

The radiance reflected by the slab in direction ν for light conically incident from the ν' direction. The reflection is normalized to an incident diffuse flux, π. This definition has the advantage that R(ν',ν) has finite non-zero values when ν = 0 or ν' = 0 and thereby improves the computational

accuracy. Furthermore, R(v',v) is the ratio of the actual reflection function to the reflection function of an ideal white Lambertian surface. The transmission function is defined similarly.

With total transmission and reflection defined, the reflected intensity distribution, I_{ref} is:

$$I_{ref}(v) = \int_0^1 I_{in}(v')R(v',v)2v'dv' \qquad \text{A1.4}$$

where I_{in} is the intensity of the incident light and R(v',v) is the reflected light. $I_{ref}(v)$ has units of power per unit solid angle. Total reflection for normal irradiance (R_c) and diffuse irradiance (R_d), and the total transmission from collimated irradiance (T_c) and diffuse irradiance (T_d) are derived by van de Hulst and Prahl as follows[32]:

$$R_c = \iint_0^1 R(v',v)\frac{\delta(1-v')}{2v'}2v'dv'2vdv = \int_0^1 R(1,v)2vdv \qquad \text{A1.5}$$

$$R_d = \iint_0^1 R(v',v)2v'dv'2vdv \qquad \text{A1.6}$$

$$T_c = \int_0^1 T(1,v)2vdv \qquad \text{A1.7}$$

$$T_d = \iint_0^1 T(v',v)2v'dv'2vdv \qquad \text{A1.8}$$

At each point within tissue, energy is lost due to absorption and scattering and gained from energy flow from surrounding areas. The radiative transport equation, RTE, is difficult to solve and requires constraints on the sample to exactly match assumptions made for an exact solution. Because of these constraints the RTE is often approximated.

Inverse adding doubling is a method that quickly and accurately approximates the RTE. Commonly the RTE is approximated using spherical harmonics. Such a method leads to a simplified system of $(N+1)^2$ connected differential partial derivative equations known as the P_N approximation. The P_N approximation has been shown to be sufficiently accurate and used in multiple studies to calculate tissue optical properties.[94-100] IAD uses quadriture which has been found to be equivalent to the spherical harmonic and P_N method of order P_{N-1}…ie four quadriture points is equivalent to a P_3 approximation.

Quadrature

Quadrature is synonymous with integration. Quadrature is a method that discretizes an integral and uses summation to approximate that integral. For example the total reflection for normal irradiance (R_c) is given by:

$$Rc = \int_0^1 R(1,v)2vdv \qquad \text{A1.9}$$

This integral can be approximated using quadrature using the identity:

$$\int_a^b f(x)g(x)dx \approx \sum_{i=1}^{M} f(x_i)w_i \qquad \text{A1.10}$$

thus…

$$\int_0^1 R(1,\nu)2\nu d\nu \approx \sum_{i=1}^{M} 2\nu_i w_i R_{iM} \qquad \text{A1.11}$$

The integration points x_i and w_i are chosen so the integration will integrate a polynomial of degree 2M exactly.

An example of quadriture use in IAD is as follows[32]:

Consider a homogenous slab with a fixed albedo (a= 0.9), isotropic scattering (g=0) and an optical thickness (τ=1). With an infinitely wide incident light on a slab the reflected light will vary with exit angle. Quadrature was used by Prahl[32] to solve the above reflectance integral which gives the angular dependant reflection as:

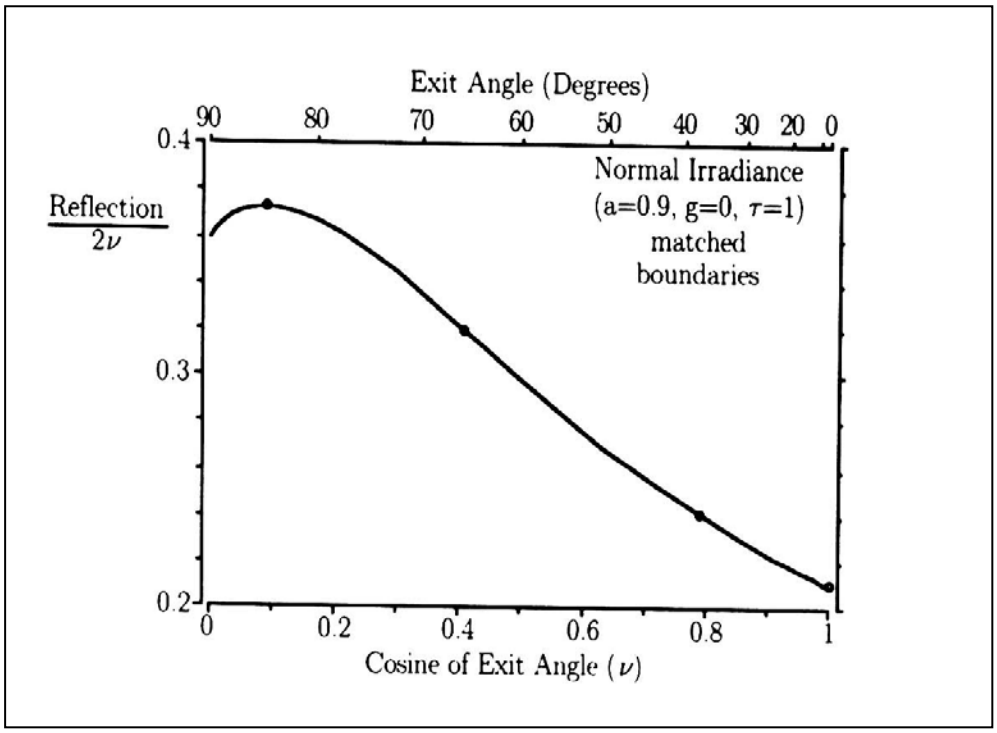

Each dot represents a point of quadrature. Note that the percent reflectance at each angle is given. For a P_3 equivalent spherical harmonic approximation, four quadrature points are used in the IAD program to approximate the angular dependant total reflection. Transmission values are calculated similarly. Four quadrature points was found to give an error of 2-3 %. Increasing the number of quadrature points more accurately approximates the solid line in the graph above and leads to a decrease in error. For example 36 quadrature points was found to have an error of on 0.1%.

Uniqueness

The IAD method continually guesses the optical coefficients until the calculated transmission and reflectance values match the experimental values. It is not obvious that the IAD calculated optical coefficients (a, τ, g) are unique for a set of measurements (R_T, T_T, T_c). For example increasing the albedo ($a = \mu_s/(\mu_a + \mu_s)$) of a sample will increase its total reflection and minimize the transmission…and increasing the optical thickness of the sample (τ) will do the same. Prahl demonstrated the uniqueness of IAD calculated optical properties for two conditions: 1) fixed unscattered transmission and 2) fixed scattering anisotropy.[31] For each case the optical coefficients were found to be unique with only one existing set of optical coefficients leading to the measured transmission and reflection with an assumed anisotropy factor (g).

Errors

Prahl also examined the accuracy of the IAD method.[31] The error analysis was conducted numerically because analytical expressions for light propagation in anisotropic media with mismatched boundaries were not available. Using four quadrature points the error consistently was found to be 2-3 % when compared to Monte Carlo modeling of light propagation through tissue. Increasing the number of quadrature points improved accuracy at the cost of computational time. The 36 quadrature point simulation was within 0.1 % accurate of the Monte Carlo values. The finding suggest the IAD method to be an accurate and time efficient method of calculating the optical properties of tissues.

APPENDIX B

NONLINEAR OPTICS

Nonlinear Optical Phenomena describe the nonlinear response of a material system to an applied electric field and is described by the polarization equation.

$$P(t) = \chi^{(1)}E(t) + \chi^{(2)}E(t)E(t) + \chi^{(3)}E(t)E(t)E(t) + \ldots \quad \text{A2.1}$$

where χ is the optical susceptibility and characterizes the material response to an applied electric field, E(t). The first term is a linear term describing events such as light absorption and scattering. Second harmonic generation (SHG), the signal imaged in the study to examine collagen structure, stems from the second term in the polarization equation:

$$\chi^{(2)}E(t)E(t) \quad \text{A2.2}$$

For convenience the nonlinear susceptibility and electric fields will be discussed separately.

Electric Field Interactions

SHG is a frequency doubling effect. Consider an electric field with strength:

$$E(t) = Ee^{-i\omega t} + c.c. \qquad \text{A2.3}$$

where "c.c." is the complex conjugate. The second term consists of two electric fields interacting so multiplying E(t) x E(t) we have:

$$E(t) \times E(t) = \left(Ee^{-iwt} + c.c.\right)\left(Ee^{-iwt} + c.c.\right) =$$

$$E^2e^{-2wt} + E + E^* + E^2e^{2wt} = 2EE^* + (E^2e^{-2wt} + c.c.) \qquad \text{A2.4}$$

Notice when the two electric fields are multiplied together we are left with a time independent term, $2EE^*$, and a time dependant, frequency doubled term that is responsible for producing second harmonic signal, E^2e^{-2wt}.

Optical Susceptibility

There are strict material characteristics for second harmonic generation. Two major criteria are: 1) the medium must be highly organized and be on a size scale similar or larger than the wavelength of incident light and 2) the medium must lack a center of inversion. The optical susceptibility, χ, is a third rank tensor representation of these material properties. $X^{(2)}_{ijk}$ is represented by three, 3x3 matrices. For SHG, dispersion can be neglected so the following shorthand was developed:

$X^{(2)}_{ijk}=$

$$\begin{bmatrix} 111 & 112 & 113 \\ 121 & 122 & 123 \\ 131 & 132 & 133 \end{bmatrix} \begin{bmatrix} 211 & 212 & 213 \\ 221 & 222 & 223 \\ 231 & 232 & 233 \end{bmatrix} \begin{bmatrix} 311 & 312 & 313 \\ 321 & 322 & 323 \\ 331 & 332 & 333 \end{bmatrix}$$

Because of symmetry:

123 = 132, 223 = 232, 323 = 332

131 = 113, 231 = 213, 331 = 313

112 = 121, 212 = 221, 312 = 321

The new shorthand matrix (d_{il}) becomes:

$$d_{il} = \begin{bmatrix} d_{11} & d_{12} & d_{13} & d_{14} & d_{15} & d_{16} \\ d_{21} & d_{22} & d_{23} & d_{24} & d_{25} & d_{26} \\ d_{31} & d_{32} & d_{33} & d_{34} & d_{35} & d_{36} \end{bmatrix}$$

If the medium has a center of inversion all components of the matrix become 0 and no SHG is produced. Collagen lacks a center of inversion and therefore produces SHG signal with a sufficiently intense laser light source. The optical susceptibility matrix describing SHG for rat tail collagen is[101]:

$$d = \begin{bmatrix} 0 & 0 & 0 & 0 & 0 & d_{16} \\ d_{21} & d_{22} & d_{23} & 0 & 0 & 0 \\ 0 & 0 & 0 & d_{34} & 0 & 0 \end{bmatrix}$$

APPENDIX C

SPECTROPHOTOMETRY, OPTICAL ABSORPTION

Absorption spectroscopy in the UV and visible range is an important tool in identifying and quantifying chemicals. Spectrophotometry was implemented in this dissertation as a way to measure the quantity changes of soluble collagen in solution before and after fibrillogenesis.

The Beer-Lambert law describing absorption is the mathematical basis for spectrophotometry. Light is absorbed as it passes through a transparent material. The extinction of light is described by[102]:

$$\log\left(\frac{I_0}{I}\right) \equiv A_v = (\varepsilon_v)cd \qquad \text{A3.1}$$

where A_v is the absorbance, I_0 is the intensity of monochromatic light entering the sample, I is the intensity of light emerging from the sample, d is the path length, c is the concentration of absorbing substance, and ε_v is the molar extinction coefficient. ε_v is wavelength dependant and is a characteristic of the substance whose absorption is being measured. In spectrophotometry the absorbance of a range of wavelengths is measured for a chemical solution.

APPENDIX D

RAMAN SCATTERING

The following is a more in depth mathematical description of Raman scattering from Ewen Smith and Geoffrey Dent's book entitled, "Modern Raman Spectroscopy: A Practical Approach."[103] This is not an exhaustive description, but a description aimed at understanding major concepts useful for the experimentalist to understand. For a more in depth discussion the reader should be directed to the many published books on the subject.[104-105]

Raman spectroscopy is fundamentally based on Raman scattering. Earlier, light scattering was described as emitted light resulting from the interaction of an incident light wave and matter. When light interacts with particles such as molecules that are smaller than its wavelength three types of scattering events result:

1. Rayleigh scattering – Elastic scattering event where emitted light is same frequency as incident light.
2. Stokes Raman Scattering – Inelastic scattering event where emitted light is of a lower frequency than the incident light.
3. Anti-Stokes Raman Scattering – Inelastic scattering event where emitted light is of a higher frequency than incident light.

Below is a brief discussion of the major components of Raman scattering:

Vibrational states and Hooke's Law

Molecules consists of electronic states which each contain a large number of vibrational and rotational states. A typical diagram of an electric state consisting of vibration levels is as follows and will be referred to as a Morse diagram:

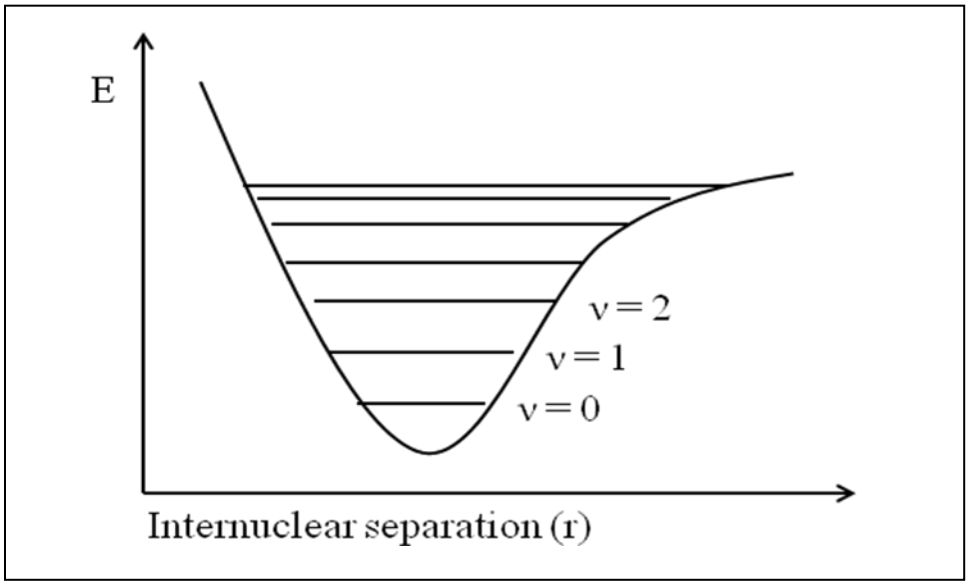

The y-axis represents the energy of the system with the x-axis representing the distance between two atomic nuclei. The curved line indicates the electronic state whereas straight lines indicate different vibrational states. Energy is quantized with vibrational states occurring at discrete energy levels. $\nu = 0$, indicates the ground state where the molecule is not vibrating. $\nu = 1$ is the first level of higher energy than the ground state and the molecule vibrates.

The Raman scattering effect results from the interaction of incident light and electrons in the illuminated molecules. In non-resonant Raman scattering, the incident light does not have enough energy to excite the electron into a higher electronic energy level. Thus the electron is promoted to a different vibrational level within the same electronic state.

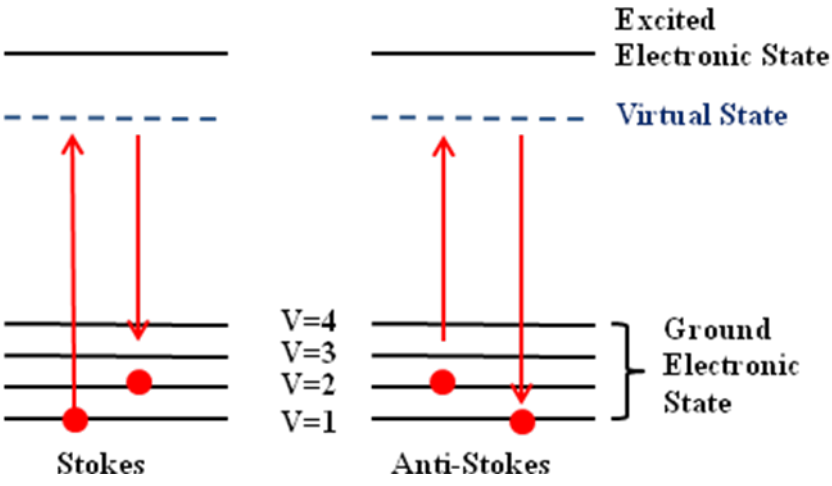

Energy diagram of inelastic Raman scattering. Scattered light energy is either lower (Stokes) or higher (Anti-Stokes) than incident light.

In order for a molecule to exhibit the Raman effect the incident light must induce a dipole moment in the molecule or induce a change in molecular polarizability. Light scattered through the Raman process can be either lower or higher energy than the light incident on the molecule. When a molecule interacts with an incident photon, some of the electrons in the molecule convert the light energy into vibrational energy. The scattered light loses energy equivalent to the change in vibrational mode (Stokes Raman

effect). If the electron is already in an elevated vibrational state, energy is donated, increasing the overall energy of the scattered photon (Anti-Skokes Raman effect). It is important to remember that the majority of scattered light is of the same energy as the incident photon (Rayleigh Scattering) with Raman scattering lines potentially only 10^{-6} of the intensity of the Rayleigh line.

The energy between vibronic levels can be calculated using a harmonic simplification of the above Morse curve. In the harmonic approximation a parabola is used rather than the non-symectric Morse curve. Also in the harmonic model the vibronic levels remain equal distant apart as energy increases. In reality however as energy increases the vibration energy levels become closer together.

The harmonic model for a diatomic molecule can be considered as two masses connected by a vibrating spring. Hooke's law can be used to give the relationship between frequency, the mass of the atoms involved in the vibration, and bond strength:

$$\nu = \frac{1}{2\pi c}\sqrt{\frac{K}{\mu}} \qquad \text{A4.1}$$

where c is the speed of light, K is the force constant of the bond, and π is the reduced mass of the two atoms (we'll call them atom "A" and "B").

$$\mu = \frac{M_A M_B}{M_A + M_B} \qquad \text{A4.2}$$

From Hooke's law we can understand some general trends:

- The lighter the atoms involved…the higher the frequency
- The stronger the bond…the higher the frequency

Polarization

Raman scattering is affected by the polarization of the incident light. Linearly polarized light is common in Raman spectroscopy and will be discussed here.

The electron cloud of a molecule can only be distorted by incident light by an amount related to the molecule's electrons ability to polarize. The amount of distortion is called the polarizability (α). The incident light is only polarized in one plane, however the electron cloud is distorted in all directions. The simple expression used to denote a molecular dipole (μ) is:

$$\mu = \alpha E \qquad \text{A4.3}$$

where E is the electric field of the incident photon. Expanding for all directions (x, y, z) we have:

$$\begin{bmatrix} \mu_x \\ \mu_y \\ \mu_z \end{bmatrix} = \begin{bmatrix} \mu_{xx} & \mu_{xy} & \mu_{xz} \\ \mu_{yx} & \mu_{yy} & \mu_{yz} \\ \mu_{zx} & \mu_{zy} & \mu_{zz} \end{bmatrix} \begin{bmatrix} E_x \\ E_y \\ E_z \end{bmatrix}$$

The above equation shows that the polarization of Raman scattered light is dependent on the polarization of incident light.

The Kramer Heiseneberg Dirac Expression

The intensity of Raman scattering is defined by:

$$I = Kl\alpha^2\omega^4 \qquad \text{A4.4}$$

K is a constant, l is the laser power, ω is the frequency of the incident radiation, and α the polarizability of the electrons in the molecule. To calculate the polarizability of the molecule the Kramer-Heisenberg-Dirac expression is used:

$$\left(\alpha_{\rho\sigma}\right)_{GF} = k\sum_I \left(\frac{\langle F|r_\rho|I\rangle\langle I|r_\sigma|G\rangle}{\omega_{GI}-\omega_L-i\Gamma_I} + \frac{\langle I|r_\rho|G\rangle\langle F|r_\sigma|I\rangle}{\omega_{IF}+\omega_L-i\Gamma_I}\right) \qquad \text{A4.5}$$

α is the molecular polarizability, ρ and σ are the incident and scattered polarizations, Σ is the sum over all vibration states of the molecule, G is the ground vibronic state, I is the vibronic state of the "excited" state, and F is the final vibronic state. Put another way, G and F are just the initial and final vibronic states which are shown in the above energy diagram of the Raman process. ω_{GI} is the energy difference between the ground state vibronic energy and the intermediate state. ω_L is the energy of the exciting light and $i\Gamma_I$ is a small error term related to the lifetime of the excited state and the breadth of Raman lines.

The numerator in the above equation shows integrals in the "bra-ket" form. They are terms that "mix" the ground and excited states in order to describe the electron configuration that has been distorted by the incident light. For example, consider the

first term describing a molecule in the ground state being excited into a higher final state:

$$\langle F|r_\rho|I\rangle\langle I|r_\sigma|G\rangle \qquad \text{A4.6}$$

Starting from the right side of the above expression, $|G\rangle$ is a wave function describing the ground vibronic state that is being acted on by the dipole opporator, r_ρ. This product is then multiplied by a wave function describing the "excited" vibronic state $\langle I|$. This in effect "mixes" the states with the result being summed (integrated) over all states.

We have just described the molecule being "excited" into a virtual state and have yet to describe the molecule returning to the final state. A similar process as just describes happens in the left side of the above equation and the molecule is left in the final state $\langle F|$.

The process just described does not have to start in the ground state. For example electrons could reside in high vibrational states if the molecules have sufficient heat energy. The second "bra-ket" term in the Kramer-Heisenberg-Dirac (KHD) expression accounts for this case. Consider:

$$\langle I|r_\rho|G\rangle\langle F|r_\sigma|I\rangle \qquad \text{A4.7}$$

This term starts with the excited states and mixes the ground and final state together in a similar way to the previous term just described.

VITA

Jason M. Hirshburg

Address:

337 Zachry Engineering Center

3120 TAMU

College Station, TX 77843

jason.hirshburg@neo.tamu.edu

Education:

Bachelor of Engineering (May 2004), Biomedical Engineering

Vanderbilt University, Nashville, TN 37240

Doctor of Philosophy (December 2009), Biomedical Engineering

Texas A&M University, College Station, TX 77843